Prokaryotic diversity and activity in contrasting productivity regimes in late summer in the Kerguelen region (Southern Ocean)

Alejandra Elisa Hernandez-Magana, Yan Liu, Pavla Debeljak, Olivier Crispi, Barbara Marie, Coco Koedooder, Ingrid Obernosterer

Prokaryotic diversity and activity in contrasting productivity regimes in late summer in the Kerguelen region (Southern Ocean)

Alejandra Elisa Hernandez-Magana [1,2]*, Yan Liu [1, 3]*, Pavla Debeljak[1,4†], Olivier Crispi[1], Barbara Marie[1], Coco Koedooder[1]‡, Ingrid Obernosterer[1#]

[1] Sorbonne Université, CNRS, Laboratoire d'Océanographie Microbienne, LOMIC, F-66650, Banyuls/mer, France.

[2] Nordcee, Department of Biology, University of Southern Denmark, Odense M, Denmark

[3] School of Life Sciences, Ludong University, Yantai, China

[4] University of Vienna, Department of Functional and Evolutionary Ecology, A-1090 Vienna, Austria

present affiliation

[†] Institut de Systématique, Évolution, Biodiversité (ISYEB), Muséum National d'Histoire Naturelle, CNRS, Sorbonne Université

‡The Fredy and Nadine Herrmann Institute of Earth Sciences, Hebrew University of Jerusalem, Jerusalem, Israel

*These authors contributed equally to this study.

[#] Corresponding author: Ingrid Obernosterer, Microbial Oceanography Laboratory (LOMIC), CNRS-Sorbonne University, 1 Avenue Pierre Fabre, 66650 Banyuls sur mer, France.

Tel: (+33) 04 68 88 73 53

e-mail: ingrid.obernosterer@obs-banyuls.fr

Keywords: prokaryotic community composition, 16S rRNA, amplicon sequence variants, natural iron fertilization, Southern Ocean

Abstract

Natural iron (Fe) fertilization sustains phytoplankton blooms above the Kerguelen plateau (Indian sector of the Southern Ocean) within otherwise low productive off-plateau waters. In early spring and summer, these diatom-dominated blooms are associated with distinct heterotrophic prokaryotic communities, but whether a structuring effect extends to the post-bloom period has thus far not been investigated. To address this question, we carried out a detailed study of the prokaryotic community composition in the region of Kerguelen Island during late Austral summer (18 February to 27 March 2018; MOBYDICK project). Concentrations of chlorophyll *a* were seasonally low above the plateau (0.27-0.58 µg Chl *a* L^{-1}) and in a similar range to those at the 3 off-plateau sites investigated (0.14-0.34 µg Chl *a* L^{-1}), but we observed an accumulation of dissolved organic carbon and the build-up of heterotrophic prokaryotic biomass in Kerguelen plateau waters. Illumina sequencing of the 16S rRNA gene revealed that the total (DNA-based) and potentially active (RNA-based) prokaryotic communities were structured according to on- and off-plateau sites in the wind-mixed surface layer, in both the free-living (< 0.8 µm size fraction) and particle-attached (> 0.8 µm size fraction) size fractions. The Amplicon Sequence Variants (ASV) with significantly higher relative abundances in on-plateau surface waters as compared to off-plateau waters belonged to *Halieaceae* OM60 group, several *Flavobacteriaceae*, such as the NS5 marine group, *Aurantivirga* and *Ulvibacter*, *Rhodobacteraceae Loktanella*, *Saprospiraceae*, and the *Cryomorphaceae* NS10 marine group. ASVs with higher relative abundances in off-plateau waters belonged to the *Flavobacteriaceae Formosa*, the *Rhodobacteraceae Planktomarina* and the SAR11 clade. We discuss the potential abiotic and biotic drivers of community composition in late Austral summer and the ecological roles of abundant prokaryotic taxa in Kerguelen plateau waters.

1. Introduction

Heterotrophic prokaryotes contribute to the cycling of all elements in the ocean. Within the marine carbon cycle, they process roughly half of recent primary production with most of the organic carbon being respired (Ducklow *et al.*, 2007). This process mediates large fluxes of carbon and energy between autotrophic and heterotrophic microbial communities and has important consequences for the potential storage of carbon in the ocean interior by the biological pump. Phytoplankton blooms are seasonally re-occurring events that stimulate prokaryotic and higher trophic level growth and metabolic activity. Diverse prokaryotes carry out the transformation of phytoplankton-derived organic matter (reviewed in Buchan *et al.*, (2014)) and the response is generally most pronounced a few weeks after the peak in phytoplankton biomass (Bunse and Pinhassi, 2017). The observed succession in prokaryotic communities over the course of phytoplankton blooms (Teeling *et al.*, 2012) illustrates the dynamic interplay between the composition of organic matter released by phototrophs, the metabolic capabilities of individual taxa, and the potential species-specific phytoplankton-prokaryote associations.

Phytoplankton blooms induced by natural iron (Fe) fertilization provide excellent opportunities to investigate these processes in the otherwise low-productive Southern Ocean. The region east of Kerguelen Island harbors the largest phytoplankton blooms induced by natural Fe fertilization (Blain *et al.*, 2007). Prokaryotes contribute substantially to the transformation of phytoplankton-derived organic matter during early spring (November), summer (January-February) and late summer (February-March) corresponding to the onset, peak and early decline, and the post-bloom phases in these perennially cold waters (Christaki *et al.*, 2020). These diatom-dominated blooms (Armand *et al.*, 2008; Lasbleiz *et al.*, 2016; Blain *et al.*, 2020) are associated with prokaryotic heterotrophic communities during early spring (Landa *et al.*, 2016) and in summer (West *et al.*, 2008; Obernosterer *et al.*, 2011) that

are distinct to those in surrounding low-productive waters. Onboard experiments have highlighted the role of diatom-derived organic matter in shaping prokaryotic community composition in spring (Landa *et al.*, 2016), and potential associations between diatom species and prokaryotic taxa has been identified as mechanism for the temporal structuring of microbial communities (Liu *et al.*, 2020). Observations from the post-bloom period when phytoplankton biomass has similar levels in on and off-plateau waters are thus far lacking, preventing to address the question on the effects Fe-fertilization on prokaryotic community composition at the seasonal scale in the Southern Ocean.

Numerous studies have described prokaryotic communities in different size-fractions, considered as free-living and particle-attached prokaryotes. The diversity and specific metabolic activity was shown to be higher in communities attached to particles as compared to free-living ones (Ghiglione *et al.,* 2007, Zhang et al., 2007; Ortega-Retuerta *et al.,* 2013; Rieck *et al.,* 2015; Zhang *et al.,* 2020) or unchanged between size-fractions (Bachmann et al., 2018). Observed differences have been associated to the respective lifestyle and metabolic capabilities. The composition, origin and quality of the particles was shown to have a strong influence on the associated prokaryotes (Zhang *et al.,* 2007; Ortega-Retuerta *et al.,* 2013; Rieck *et al.,* 2015). Therefore, exploring the free-living and particle-attached community structure can provide a better understanding of the processes influencing the prokaryotic diversity.

The present study was carried out as part of the project MOBYDICK (Marine Ecosystem Biodiversity and Dynamics of Carbon around Kerguelen: an integrated view) that aimed to provide a detailed picture of the diversity and role in the carbon cycling of biological communities of end-to-end food webs in contrasting nutrient regimes in the Southern Ocean. Our specific objective was to provide a description of the prokaryotic community composition. We considered the total (DNA-based) and potentially active (RNA-based) free-

living (<0.8 μm) and particle-attached (>0.8 μm) prokaryotic communities in the upper 300 m water column. Our observations from late Austral summer, corresponding to roughly 2 months after the peak of the phytoplankton bloom, reveal distinct prokaryotic communities in Kerguelen plateau surface waters as compared to off-plateau waters. We further identified the prokaryotic taxa that explained the differences between on- and off- plateau waters, providing insights to microbial processes occurring during post-bloom conditions in this fertilized region of the Southern Ocean.

2. Material & Methods

2.1. Study area

Samples were collected in the region of Kerguelen Island in the Indian Sector of the Southern Ocean in late Austral summer (MOBYDICK cruise; February 18 to March 27, 2018) (Fig. 1). Four stations, identified as MOBYDICK-1 (M1), M2, M3 and M4 were sampled (Table 1). Station M2 is located on the central Kerguelen plateau (overall depth 527 m), southeast of Kerguelen Island, in naturally Fe-fertilized waters (Blain *et al.*, 2007). The other three stations are located in off-plateau waters, east (M1) and southwest of Kerguelen Island (M3 and M4). Station M3 is located in the polar frontal zone and stations M1, M2 and M4 are in Antarctic waters, with station M1 being strongly influenced by the polar front (Pauthenet *et al.*, 2018). The sampling period during the MOBYDICK cruise corresponded to roughly two months after the seasonal maximum in chlorophyll *a* (Chl *a*) concentrations in on- and off-plateau waters (Fig. S1). Station M2 was sampled three times (M2-1, M2-2 and M2-3) in an eight-day interval, stations M3 (M3-1 and M3-3) and M4 (M4-1 and M4-2) were each sampled twice with a 14-day interval and station M1 was visited once (Table 1).

2.2. Sample collection

Seawater samples were collected with 12 L Niskin bottles mounted on a rosette equipped with a conductivity, temperature, depth sensor (Seabird SBE-911 plus CTD unit). Discrete samples for concentrations of Chl *a* and dissolved organic carbon (DOC), and prokaryotic abundances were taken at 10 to 12 depths in the upper 500m. The sampling depths for prokaryotic community composition were chosen according to the CTD profiles with the aim to collect seawater at the top and at the base of the surface mixed layer (Z_{ML}), in the transition layer, and in deeper waters (Fig. S2). We used this strategy to obtain 2 samples from the Z_{ML}, focus of our study, and to allow for a comparison of the surface water communities with those from deeper layers. Seawater samples were collected at 10m, 60m, 125m and 300m at all sites and visits, except for M2-1, where the following depths were sampled 10m, 50m, 100m and 300m. For clarity, the 50 m and 100m sampling depths at station M2-1 will be referred to 60 m and 125 m, respectively, in the description of the results and figures. The samples collected at the two uppermost depths were within the Z_{ML} at all sites and visits, except for Station M1 where only the uppermost depth was within the shallow Z_{ML} (Table 1).

2.3. Concentration of Chl *a*

For the analysis of Chl *a* concentrations, 2.32 L of seawater were filtered through Whatman GF/F filters and the filters were stored in liquid nitrogen until analysis in the laboratory. Filters were extracted in 100% methanol, disrupted by sonication and clarified by GF/F filtration after 2h. Samples were analysed within 24h using High Performance Liquid Chromatography on an Agilent Technologies HPLC 1200 system equipped with a diode array detector following (Ras *et al.*, 2008).

2.4. Dissolved organic carbon

The concentration of dissolved organic carbon (DOC) was determined in samples filtered through two combusted (450°C, 4h) GF/F filters. Subsamples of 10 mL (in triplicate) were transferred to pre-combusted glass ampoules and acidified with H_3PO_4 (final pH = 2). The sealed glass ampoules were stored in the dark at room temperature until analysis. DOC measurements were performed on a Shimadzu TOC-V-CSH (Benner and Strom, 1993). Prior to injection, DOC samples were sparged with CO_2 -free air for 6 min to remove inorganic carbon. Hundred µL of each of the sample replicates were injected in triplicate and the analytical precision was 2%. Standards were prepared with acetanilide. Consensus reference materials provided in sealed glass ampoules (http://www.rsmas.miami.edu/groups/biogeochem/CRM.html) was injected every 12 to 17 samples to insure stable operating conditions.

2.5. Enumeration of heterotrophic prokaryotes

For the enumeration of heterotrophic prokaryotes by flow cytometry, subsamples (1.44 mL) were fixed with glutaraldehyde grade I 25% (1% final concentration), and incubated for 30 min at 4 °C, then quick-frozen in liquid nitrogen and stored at -80 °C until analysis. Samples were collected from unfiltered seawater, considered as the bulk prokaryotic abundance, and from the < 0.8 µm size fraction, considered as the abundance of free-living prokaryotes. Samples were thawed at room temperature. Counts were performed on a FACSCanto II flow cytometer (Becton Dickinson) equipped with 3 air-cooled lasers: blue (argon 488 nm), red (633 nm) and violet (407 nm). For the enumeration of non-autofluorescent cells, mainly heterotrophic prokaryotes, cells were stained with SYBR Green I (Invitrogen – Molecular Probes) at 0.025% (vol / vol) final concentration for 15 min at room temperature in the dark. Stained prokaryotic cells were discriminated and enumerated according to their right-angle

light scatter (SSC) and green fluorescence at 530/30 nm. In a plot of green versus red fluorescence, non-autofluorescent cells were distinguished from autofluorescent cells. Fluorescent beads (1.002 µm; Polysciences Europe) were systematically added to each analyzed sample as internal standard. The cell abundance was determined from the flow rate, which was calculated with TruCount beads (BD biosciences).

2.6. Prokaryotic community composition

For the analysis of prokaryotic community composition, seawater was passed through a 60 µm nylon mesh and 6 L of seawater was filtered through 0.8 µm pore-size polycarbonate (PC) membranes (47 mm diameter, Nuclepore, Whatman, Sigma Aldrich, St Louis, MO) to retrieve the particle-attached (>0.8 µm) fraction. Prokaryotic cells in the < 0.8 µm fraction were concentrated on 0.22 µm cartridges (Sterivex™ Millipore, EMD, Billerica, MA) and considered as free-living fraction. The filters were stored in sterile Eppendorf tubes (2 ml) and the cartridges were sealed at both ends using parafilm. The filters and cartridges were stored at -80° C until DNA and RNA extraction.

DNA and RNA extractions were performed simultaneously from the PC membranes (> 0.8 µm fraction) and the Sterivex™ cartridges (> 0.2 µm fraction) respectively, using the AllPrep Kit (Qiagen, Hilden, Germany) as described in (Liu *et al.*, 2019) with minor modifications. The filter units were thawed and closed with a sterile pipette tip end at the outflow, 425 µl lysis buffer were added per sample (40mM EDTA, 50mM Tris and 0.75 M sucrose) and three freeze-thaw cycles were performed with liquid nitrogen and a water bath at 65°C. Subsequently, 25µl of freshly prepared lysozyme solution were added (2 mg ml^{-1} final concentration), the filter units were placed in a rotary mixer and incubated at 37°C during 45 minutes, and then 8µl of proteinase K solution (0.2 mg ml^{-1} final concentration) and sodium

dodecyl sulphate (SDS) (1%) were added and maintained at 55°C with gentle agitation every 10 min for 2 hrs.

To protect the RNA, 10 µl of β-mercaptoethanol were added to 1 ml of RLT plus buffer provided by the kit, 1,550 µl of this solution were added to each filter unit and mixed by inversion. The lysate was recovered by using a sterile 5 ml syringe and loaded in three additions onto the DNA columns by centrifuging at 10 000g for 30 s. DNA and RNA purifications were performed following the manufacturer's guidelines (Qiagen, Germany). The Invitrogen™ SuperScript™ VILO™ cDNA Synthesis Kit (Thermo Fisher Scientific Inc. Carlsbad, CA USA) was utilized to generate cDNA from the RNA extracts. Prior to the reverse transcription, absence of DNA in the RNA extracts was verified by PCR test with general primer sets 341F (5'-CCTACGGGNGGCWGCAG) and 805R (5'-GACTACHVGGGTATCTAATCC) (Herlemann *et al.*, 2011) for the prokaryotic 16S rRNA gene, followed by the examination of amplification products on 1% agarose gel electrophoresis. If a specific band of 1 015 bp was observed the RNA extract was treated with DNase.

The final PCR amplification of DNA and cDNA extracts was performed using the primers 515F-Y (5′-GTGYCAGCMGCCGCGG TAA) and 926R (5′-CCGYCAATTYMTTTRAGTTT) that encompasses the V4 and V5 hypervariable regions of the 16S rDNA (Parada *et al.*, 2016). Triplicate 10 µl reaction mixtures contained 2 µg DNA, 5 µl KAPA2G Fast HotStart ReadyMix, 0.2 µM forward primer and 0.2 µM reverse primer. PCR amplification was performed under the following conditions: an initial denaturation step of 95°C for 3 min, followed by 30 cycles of denaturation at 95°C for 45 s, annealing at 50°C for 45 s, and extension at 68°C for 90 s, and a final elongation step at 68°C for 5 minutes.

The presence of amplification products was confirmed by 1% agarose electrophoresis and PCR triplicates were pooled and purified by gel-filtration through-Sephadex G-50 Super Fine resin (Amersham Biosciences, Uppsala, Sweden). Then the purified samples were recovered for sequencing. The 16S rRNA gene amplicons were sequenced via next generation sequencing (Illumina MiSeq 2 × 250 bp chemistry on one flow-cell) at the platform GeT-PlaGe Genotoul (Toulouse, France). Mock community DNA (LGC standards, UK) was used as a standard for subsequent analyses and considered as a DNA sample for all treatments. In total, 128 samples (32 DNA free-living, 32 DNA particle-attached, 32 cDNA free-living and 32 DNA particle-attached) were sequenced. After the sequencing one sample (cDNA free-living at M2_1-60m) was discarded, due to low quality in the sequencing.

2.7. Sequence analysis

The samples obtained in the sequencing run were demultiplexed at the platform GeT-PlaGe Genotoul (Toulouse, France). A total of 5,847,892 sequences were obtained. Processing sequences was conducted with the DADA2 package for R version 1.10.1 (Callahan *et al.*, 2016a), following the pipeline by (Callahan *et al.*, 2016b). Amplicon sequence variants (ASVs) were inferred through the high resolution DADA2 method (Callahan *et al.*, 2016a; Callahan *et al.*, 2017). Primers were trimmed and the sequences were filtered based on their quality using DADA2 (maxEE=2, truncQ=2). Forward reads with a length of 245 bp, reverse reads with a length of 210 pb, and in total 4,253,969 reads were kept after quality filtering. Error rates were estimated from the data, and inference of the sequence variants was made from the pooled sequences from all the samples. The 1,059,953 unique forward sequences and 1,619,348 reverse unique sequences were pooled to determine the sequence variants, then the forward and reverse sequences were merged and chimeras were removed. We obtained 31, 227 unique ASVs. Taxonomy was assigned based on the SILVA database release 132 at the highest taxonomic level possible (Quast *et al.*, 2013).

From the 5,847,892 reads we obtained a total of 14,204 ASVs for the 127 samples after singletons removal. The number of reads per sample varied between 2,803 and 48,536. The dataset was randomly subsampled to the lowest number of reads (2,803) per sample with rarefy_even_depth( ) by Phyloseq R package version 1.26.1 (McMurdie and Holmes, 2013). Ordinations were performed with both the complete and subsampled datasets, and the trends observed were consistent for both datasets. To enable the comparison between samples with different numbers of reads, we chose to carry out all analysis using the subsampled dataset. After subsampling, 12,010 ASVs remained in the dataset.

From a total of 127 samples, the prokaryotic community composition was determined in the free-living (< 0.8 μm) and in the particle-attached (> 0.8 μm) fractions. DNA-based samples represent the total prokaryotic community and RNA-based samples were used to identify the potentially active members of the community (Blazewicz *et al.*, 2013). Our sequencing data provided access to 12,010 ASVs, of which 8,871 ASVs were obtained for the free-living fraction and 8, 838 ASVs for the particle-attached fraction, and 5,699 ASVs were shared between these fractions.

In order to identify the prokaryotic taxa, the ASVs were compared against the SILVA database release 132 at the highest taxonomic level possible (Quast *et al.*, 2013). The ASVs with the same taxonomy at the order level were pooled for illustration of the relative abundance in the samples. Sequences alignment was performed using MAFFT online service for multiple sequence alignment (Katoh *et al.*, 2019) and the phylogenetic tree was built using PhyML 3.0 online program, based on the maximum likelihood method, with 100 bootstraps and the HKY85 substitution model (Guindon *et al.*, 2010). The phylogenetic tree was visualized with SeaView version 4.7 and saved as a rooted tree (Gouy *et al.*, 2010). The tree was imported in R with the ape package function read.tree( ).

To estimate the absolute cell numbers, the ASVs were corrected for copy numbers of the 16S rRNA gene per cell per specific taxa obtained from the ribosomal RNA database (Stoddard *et al.*, 2015). Total cell numbers per bacterial group and per Liter were then calculated with 16S rRNA gene relative proportions per group and total cell abundance from flow cytometry.

2.8. Data analysis

The difference between total (DNA-based) and potentially active communities (RNA-based) was tested by analysis of similarity (ANOSIM), resulting significant differences ($p=0.001$, $r=0.23$, permutations=999). Likewise free-living and particle-attached fractions for both, total (DNA) and potentially active (RNA) communities revealed significant differences ($p=0.001$, $r=0.57$, for DNA-based set and $p=0.001$, $r=0.41$ for RNA-based dataset, permutations=999). The analyses performed thereafter considers therefore separately the four subsets, free-living and particle attached fractions for both, total (DNA) and potentially active (RNA) community.

To explore the distribution patterns of the prokaryotic communities we applied Non-Metric Multidimensional Scaling (NMDS), based on the dissimilarity matrix of the community structure. The statistical analyses were performed in R 3.5.3 version (R Core Team, 2019), Bray–Curtis dissimilarity matrices were generated via vegdist( ) function using the relative abundance of ASVs in each sample. Subsequently, the matrix was used to build the NMDS ordinations using metaMDS( ) function in the package Vegan (Oksanen et al., 2019). Diversity indices were calculated with phyloseq command estimate_richness( ). ANOSIM was performed to test significant differences in microbial communities between sampling depths and among sites in the surface mixed layer.

The contribution of individual species (ASVs) to the average Bray-Curtis dissimilarity between the on- and off-plateau groups was obtained using similarity percentage analysis (SIMPER) (Clarke 1993). Station M3 was chosen as the representative off-plateau site and compared to the on-plateau station M2. The analysis was applied to the prokaryotic communities within the wind mixed surface layer. The ASVs with a relative abundance lower than 1% in at least one sample were discarded prior to the SIMPER analysis. Once the ASVs with significant contribution to the dissimilarity between groups were obtained (p-value < 0.005), the ASVs with relative abundance higher than 5% in at least one sample were selected for plotting them in a heatmap using the package pheatmap version 1.0.12 for R (Kolde, 2019).

Partial Mantel tests for the free-living and particle attached fractions in both total (DNA-based) and active (RNA-based) prokaryotic community composition, diatom community composition and environmental parameters (temperature, salinity, concentrations of dissolved oxygen, ammonium, nitrite, nitrate, phosphate, silicic acid and DOC), were performed in Vegan using mantel.partial() based on the Pearson correlation method. Prior to correlation analysis, environmental variables were z-score transformed. The amount of variance in prokaryotic community composition explained by diatoms and environmental parameters was estimated as the square of the correlation coefficient (Rho^2) based on partial Mantel test. The Partial Mantel test was applied to samples in the upper 125m water column, for which diatom community composition was available.

Redundancy analysis (RDA) (Legendre & Legendre, 2012) was applied to evaluate the linkages between the prokaryotic community composition and the environmental parameters in Vegan using rda(). Prior to analysis the environmental variables were z-score transformed

and Hellinger transformation was applied to the community matrix (Legendre & Gallagher, 2001). Permutational multivariate analysis of variance in Vegan with adonis() was used to select the significant environmental variables ($p<0.05$). We used the variance inflation factor (VIF) to determine the linear dependency among variables. We first evaluated all the variables and removed, one at a time, those with a VIF >10 from the dataset. Only the selected variables (with a VIF<10) were used to perform the final RDA analysis. As for the Partial Mantel test, samples in the upper 125m were considered.

3. Results

3.1. Environmental conditions

During late Austral summer the water column was well-stratified, with the wind-mixed surface layer (Z_{ML}) ranging between 49 m and 62 m during the first visits of the off-plateau station M4 (M4-1) and of the on-plateau station M2 (M2-1 and M2-2), respectively (Table 1 and Fig. S2). The occurrence of a storm on March 10th lead to a deepening of the Z_{ML} that was most pronounced at station M4 (87 m). A shallow Z_{ML} (27 m) was determined during our visit at station M1. Temperature in the Z_{ML} was lowest at the southernmost station M4 (4.5°C) and varied between 4.9°C (station M1) and 5.6°C (station M3-1) at the other sites (Table 1, Fig. S2). Seasonally low concentrations of Chl *a* were determined at all sites (Fig. S1), and those in the Z_{ML} of the on plateau station M2 (0.27-0.58 µg L^{-1}) were 2-3-fold higher as compared to those at the off-plateau stations M3 (0.14-0.19 µg L^{-1}) and M4 (0.18-0.21 µg L^{-1}) (Fig. 2), and similar to those at station M1 (0.34 µg L^{-1})(Chl *a,* DOC and prokaryotic abundance for station M1 are illustrated in Fig. S3). Chl *a* concentrations doubled in the Z_{ML} between the 2nd and 3rd visit at the on-plateau site M2.

Concentrations of dissolved organic carbon (DOC) were 54.1±0.6 µM in the Z_{ML} of station M2 (all visits pooled), as compared to 50.5±0.7 µM at station M3 and 50.3±0.8 µM at station M4 (Fig. 2). This accumulation of DOC is likely a consequence of the enhanced seasonal phytoplankton activity in Kerguelen plateau waters. Heterotrophic prokaryotic abundance was as high as 1.17 x 10^6 cells mL^{-1} in the Z_{ML} during our first visit of the on-plateau station M2, and cell abundances decreased to 0.81 x 10^5 cells mL^{-1} and 0.68 x 10^5 cells mL^{-1} during the following one and two weeks, respectively. Moderate (from 6.96 to 4.45 x 10^5 cells mL^{-1} at M3) and minor decreases (from 5.52 to 5.01 x 10^5 cells mL^{-1} at M4) were observed at the off-plateau stations over the 2 weeks that separated the visits (Fig. 2). The prokaryotic cell abundance in the < 0.8 µm fraction accounted for 89±11 % (n=10)(Table S1) of the abundance in unfiltered seawater in surface waters at the different sites.

3.2. Vertical and spatial structuring of prokaryotic communities

When considering the entire data set, NMDS ordination revealed a clustering by depth layer, for the total and active prokaryotic communities in both size fractions. Samples collected for the free-living fraction at 10 m and 60 m, corresponding to the Z_{ML} except for station M1 (Table 1), clustered and were distinct from those of 125 m and 300 m (Anosim, r=0.69 for DNA and r=0.61 for RNA, p=0.001) (Fig. 3a for DNA and Fig. S4a for RNA). In the case of the particle-attached fraction, the clustering by depth was less pronounced, but still significant (Anosim, r=0.58 for DNA and r=0.67 for RNA, p=0.001) (Fig. 3b for DNA and Fig. S4b for RNA). We determined multiple diversity indices that all revealed an increase with depth in both size-fractions (Table S2) as illustrated for the Shannon index on Table 2.

To identify possible differences in the prokaryotic community composition among sites, we then focused on samples collected in the Z_{ML}. For the free-living fraction, samples grouped

according to station (ANOSIM, r=0.77 for DNA and r=0.51 for RNA, p= 0.001)(Fig. 3a and Fig. 4a). This pattern was again less pronounced for the particle-attached fraction (ANOSIM, r=0.62, p=0.001 for DNA and r=0.41 p=0.006 for RNA)(Fig. 3b and Fig. S4b). Diversity of the total free-living communities was significantly lower in the Z_{ML} of the on-plateau station M2 (Shannon: 4.34±0.19 for DNA, n=6) as compared to that in off plateau waters at stations M1, M3 and M4 (Shannon: 4.86±0.15 for DNA, n=9)(one-way ANOVA $p<0.001$). This trend was, however, not observed for the potentially active free-living communities (Shannon: 5.28±0.71 at station M2 and 5.53±0.77 in the off-plateau stations, n=9) and the particle-attached communities in the DNA and RNA data sets (Table 2 and Table S2).

3.3. Prokaryotic community composition in surface waters

We further explored in more detail the prokaryotic community composition in surface waters (10 m). The total free-living and particle-attached prokaryotic communities were dominated by *Flavobacteriales* (relative contributions of 53% and 64% in on-plateau waters, 35% and 36% in off-plateau waters, respectively) and *Rhodobacterales* (20% and 10% on-plateau, 17% and 22% off-plateau, respectively). *Cellvibrionales* represented 13% in both size fractions at the on-plateau station (M2), while at the off-plateau stations this order was substantially more abundant in the particle-attached (17%) than in the free-living fraction (3%) (Fig. 4; RNA data are illustrated in Fig. S5). Distinct features of the free-living communities in off-plateau waters were the comparably higher contributions of the SAR11 clade, belonging to *Pelagibacterales* (SAR11, 17-25%), the SAR86 clade (5-8%), *Thiomicrospirales* (2-3%) and *Puniceispirillales* (2-4%). *Verrucomicrobiales* were present only in the total particle-attached communities and their relative abundances were higher in the off-plateau sites (4 - 8%) than in on-plateau waters (1.3%). *Chitinophagales* were detectable only in the particle-attached

fraction at station M2 in both the total (2.2%) and potentially active communities (3.2%), while *Sphingomonadales* (2.5%), *Lactobacillales* (1.4%) and *Ricksettsiales* (1.3%) appeared to be specific to the total particle-attached communities at station M1.

The high resolution allowed us to identify the relative contribution of the members of the prokaryotic community at the level of ASVs. Interesting information derived at this level of resolution is that in the case of some of the abundant taxonomic groups composed by multiple ASVs, only a few of them were highly abundant. For example, in the total free-living fraction (Fig. S6), *Flavobacteriales* were composed of 24 ASVs, however, only some of them were more abundant in on-plateau than in off-plateau waters. This was the case for ASV6 *Ulvibacter*, ASV12 (NS2b marine group), ASV23 (*Flavobacteriaceae* ASV15 *Aurantivirga* and ASV36 *Polaribacter*). By contrast, other *Flavobacteriales* ASVs were relatively more abundant in off-plateau waters, such as ASV3 *Formosa*, ASV38 and ASV88 (both NS7 marine group). Another interesting observation is that the most abundant ASV from our dataset, ASV1 OM60(NOR5), belonging to the gammaproteobacterial clade, was only highly abundant in the free-living fraction of the on-plateau station M2, which was not the case for the off-plateau free-living community (Fig. S6). By contrast, the same ASV was highly abundant at all sites in the particle-attached total community, and less abundant in the potentially active community (Fig. S7). Given these patterns obtained from our high resolution results of the community composition, we decided to explore which prokaryotes explained the difference among sites.

3.4. Identification of site-specific prokaryotes

To address the question of which prokaryotic taxa explained the difference in the community composition between on- and off-plateau sites (Fig. 3 and Fig. S4), we performed a Simper

analysis (permutations = 999) and selected the ASVs contributing significantly ($p<0.05$) to the differences between stations at 10 m and 60 m. Because seasonal Chl *a* concentrations were lower at M3 as compared to M4 (Fig. S1) we chose station M3 as a representative off-plateau site for the further comparison with station M2. In order to simplify the visualization of the information, we considered only highly abundant ASVs (relative abundance > 5% in at least one sample).

A total of 9 and 8 highly abundant ASVs, respectively, contributed significantly to the differences in the total (DNA) or potentially active (RNA) free-living communities between stations M2 and M3 at 10 m (Fig. 5; results for 60 m are shown in Fig. S8); among those, 5 ASVs were shared between the DNA and RNA datasets. The 9 and 8 ASVs explained each 24% and 8% of the differences among sites in the total and potentially active free-living communities, respectively. For the particle-attached communities 6 and 3 ASVs contributed significantly to the respective differences and these ASVs explained 28% and 4% of the observed variability. Two ASVs (ASV5 and ASV15) significantly contributed to the differences in both size fractions of the DNA and RNA dataset.

ASVs that had higher relative abundances at station M2 as compared to station M3 belonged to the OM60 group (NOR5 clade, *Halieaceae* ASV1), the *Flavobacteriaceae* NS5 marine group (ASV11), the genera *Aurantivirga* (ASV15) and *Ulvibacter* (ASV6), and ASV5 and ASV23 (not identified on the genus level), the *Saprospiraceae* (ASV33) and the *Cryomorphaceae* NS10 marine group (ASV52). The *Pirellulaceae* genus *Blastopirellula* (ASV8) had low relative abundances in the free-living fraction at station M2 (<0.1%) and this ASV was absent from station M3. ASVs with higher relative abundances at station M3 as compared to station M2 were the *Flavobacteriaceae* genus *Formosa* (ASV3), and the *Rhodobacteraceae* genera *Planktomarina* (ASV16) and *Loktanella* (ASV18). Contrasting patterns were observed for the SAR11 clade (ASV9) that had higher relative abundances in

the total free-living communities at station M3, but a higher contribution to the potentially active free-living communities at station M2.

3.5. Changes in the absolute abundance of major taxa

To explore the question of whether the pronounced decrease in bulk prokaryotic abundance between repeated visits at station M2 (Fig. 2) were due to changes in specific taxa, we estimated the absolute abundances of ASVs, grouped at the order level, using previously published rRNA operon copy numbers (Stoddard *et al.*, 2015). Our results reveal an increase in the abundance of SAR11 from the first to the third visit (by up to 150%) at station M2 at 10 m and a decrease in the abundance of all other considered taxa by on average 48±12% and 65±10% after one and two weeks, respectively (Fig. 6; RNA results are shown in Fig. S9).

3.6. Linking prokaryotic community composition to biotic and abiotic factors

The combined set of abiotic environmental parameters and diatom community composition, as determined by microscopic observations (Lafond *et al.*, 2020), could each explain changes in the total and potentially active prokaryotic communities in both size fractions and all depth layers ($p<0.05$; partial Mantel test; Table S3). Environmental parameters could explain 12% and 16% of the spatio-temporal changes in the total and potentially active free-living communities, respectively, and 9% and 10% of the respective particle-attached communities. Diatoms could explain 36% and 28% of the changes in the total and active free-living communities, respectively, and 20% and 14% of the total and active particle-attached communities. An additional RDA-analysis revealed a clear distinction in on and off-plateau prokaryotic communities in the Z_{ML} while samples from 125m of all sites grouped (Fig. S10). Among the environmental parameters tested (Table S4), significant predictors of the

community composition were temperature, salinity, dissolved oxygen, ammonium, nitrite and DOC. In the Z_{ML}, DOC was a significant predictor for the free-living (p=0.039) and particle-attached fraction (p=0.01), and this was the case for salinity and the communities at 125m (p=0.001 and p=0.007, respectively).

4. Discussion

We observed distinct prokaryotic communities in surface waters above the central Kerguelen plateau as compared to those in off-plateau waters during the post-bloom period in late Austral summer. These findings add to observations from early spring (Landa *et al.*, 2016) and summer (West *et al.*, 2008; Obernosterer *et al.*, 2011) corresponding to the onset, peak and early decline of the phytoplankton bloom. A similar spatial structuring was also reported for diatoms (Armand *et al.*, 2008; Lasbleiz *et al.*, 2016; Lafond *et al.*, 2020), non-diatom phytoplankton and protists (Georges *et al.*, 2014; Irion *et al.*, 2020; Sassenhagen *et al.*, 2020) during the different bloom phases, and indicates a seasonally persistent influence of natural Fe fertilization on unicellular plankton communities. We discuss in the following the potential role of abiotic and biotic factors to better understand this pattern and the role of specific taxa in the microbial cycling of elements.

4.1. Post-bloom conditions and bulk prokaryotic features

A distinct feature of the surface waters above the Kerguelen plateau in late summer is the accumulation of DOC. Both, the Partial Mantel test and RDA analysis indicated that DOC concentrations had significant influence on the prokaryotic community composition in the wind mixed surface layer (Table S3, Fig. S10). The higher DOC concentrations likely result from the seasonally enhanced autotrophic activity, the excretion of phytoplankton-derived organic matter as cells become less active when entering a senescent stage (Myklestad *et al.*,

1989; Barofsky *et al.*, 2009), and the release of DOC due to grazing (i.e. 'sloppy-feeding') (Steinberg and Landry, 2017), leading to a relief of organic carbon limitation (Obernosterer *et al.*, 2015). Besides the quantity, the composition of organic matter could differ among on- and off-plateau sites as a consequence of the varying productivity regimes and thereby contribute to shaping the community composition. The high similarity among prokaryotes at the off-plateau sites, despite their location in different water masses supports this idea.

Seasonal observations in Kerguelen plateau surface waters could provide some insights on organic matter availability and its influence on community composition. Prokaryotic growth rates determined during the post-bloom period (0.04 to 0.15 d^{-1})(Christaki *et al.*, 2020) were in the same range as those in early spring (0.025 to 0.12 d^{-1}) (Christaki *et al.*, 2014), and lower than those determined in summer (0.22 to 0.47 d^{-1}) (Christaki et al. 2008), suggesting an increase in organic matter availability during the peak and early decline of the bloom. The seasonal modifications in organic matter availability were paralleled by changes in prokaryotic diversity. In late summer, the Shannon index in Kerguelen plateau surface waters was in the same range to those determined in early spring at the same site (about 4.5), while a drop to 2.5 was observed following the peak of the spring bloom (Liu *et al.*, 2020). This latter observation points to the dominance of a few fast-growing opportunists taking advantage of the labile organic matter during the peak and just after the bloom (Liu *et al.*, 2020), while the utilization of the post-bloom organic matter pool appears to be attributable to a large number of taxa with well-defined ecological niches.

4.2. Abundant prokaryotic taxa in Kerguelen plateau waters in late summer

Flavobacteriaceae were present at all sites, but accounted for up to 53% and 63% of relative abundance of the free-living and particle-attached total community in Kerguelen plateau surface waters. Members of this family contain a diverse repertoire of enzymatic capabilities for the degradation of complex compounds, including those of phytoplankton origin

(Kappelmann *et al.*, 2019). Substrate preferences vary among taxa (Xing *et al.*, 2015; Krüger *et al.*, 2019) leading to the niche partitioning among diverse members of this family, including the late summer community in Kerguelen plateau waters (Sun *et al.,* in press). *Aurantivirga* explained differences between on- and off-plateau waters in the total and potentially active communities in both fractions. *Aurantivirga* was shown to account for about 10% throughout the summer period in Kerguelen plateau waters (Liu *et al.*, 2020). The key role of *Aurantivirga* could be explained by the high number of polysaccharide uptake loci (PULs) and the diverse substrate spectra for glycan degradation reported for members of this genus (Krüger *et al.*, 2019). On the contrary, the *Flavobacteriaceae* genus *Formosa* had higher abundances in off plateau waters, and thus appears to be adapted to a more oligotrophic-type lifestyle.

One ASV belonging to the OM60 group (*Gammprotoebacteria*, NOR5 clade, *Halielaceae*) was among the most abundant taxa of our dataset and this ASV contributed significantly to the differences in communities between on- and off plateau surface waters. This contrasts observations from November through February when the relative abundance of this group remained low (< 2%) in plateau waters (Liu *et al.*, 2020). This clade comprises aerobic anoxygenic phototrophs and members associated to aggregates where they thrive under sub-oxic conditions (Fuchs *et al.*, 2007). In the present study, this ASV was highly abundant in the total particle-attached community (DNA-based) at all sites (Fig. S8). Another interesting feature is the potential implication of members of this clade in the degradation of the sulphur compound dimethylsulfoniopropionate (DMSP) (Nowinski *et al.*, 2019; Steiner *et al.*, 2019). Kerguelen surface waters were not enriched in particulate DMSP in summer during the peak of the diatom-dominated bloom (Belviso *et al.*, 2008). However, the shift to non-diatom phytoplankton, including DMSP producers such as Haptophytes (Schoemann *et al.*, 2005),

dominated by *Phaeocystis Antarctica* in the study region (Irion *et al.*, 2020) could suggest a different scenario in late summer. The changes in the late summer light regime due to the low phytoplankton biomass in the well-stratified shallow surface mixed layer and changes in organic carbon sources provided by non-diatom phytoplankton could have led to the success of the OM60 group. One ASV belonging to *Saprospiraceae* (*Chitinophagales*) was highly abundant in the particle-attached community, but accounted for <1% on a seasonal scale (Liu *et al.*, 2020). *Saprospiraceae* were shown to respond in terms of relative abundance in incubation experiments enriched in alginate particles (Mitulla *et al.*, 2016). The associated glycolytic abilities could be advantageous for members of this family in the occupation of a specific substrate niche, provided for example by aggregates of detrital and non-living cells that contributed to up to 65% to total particulate organic carbon in late summer in Kerguelen plateau surface waters (Lafond *et al.*, 2020).

4.3. Potential role of biotic interactions in shaping community composition

Diatom assemblages explained a substantial part of the changes in prokaryotic community composition, despite their lower biomass as compared to other bloom phases (Irion *et al.*, 2020; Lafond *et al.*, 2020). Diatoms were shown to be drivers of the prokaryotic community composition in the Southern Ocean on spatial (Liu *et al.*, 2019) and seasonal scales (Liu *et al.*, 2020), with diatom-derived DOM playing an important role in spring (Landa *et al.*, 2016). In late Austral summer, *Corethron inerme* accounted for 60-80% of total diatom biomass and it was among the most actively silicifying species in on-plateau waters (Lafond *et al.*, 2020). On a seasonal scale, *C. inerme* had a large number of positive correlations with free-living and attached prokaryotes in Kerguelen plateau waters (Liu *et al.*, 2020). These included taxa identified in the present study as being more abundant in on-plateau waters, in particular those belonging to *Flavobacteriaceae* and *Cryomorphaceae*. Another diatom abundant in Austral

summer in the study region is *Rhizosolenia* spp. (Armand *et al.*, 2008; Blain *et al.*, 2020; Lafond *et al.*, 2020). This diatom revealed strong positive correlations with the *Roseobacter* genus *Loktanella* (Liu *et al.*, 2020), a taxon that was highly abundant in off-plateau waters in the particle-attached fraction in the present study. *Corethron* spp. and *Rhizosolenia* spp. are both large diatoms (about 20 µm equivalent spherical radius, ESR), and could thus present habitats for taxa with a particle-attached lifestyle.

The marked decrease in bulk prokaryotic abundances during the consecutive visits at the on-plateau station was predominantly due to grazing by heterotrophic nanoflagellates (Christaki *et al.*, 2020). This raises the question of whether selective ingestion could have influenced prokaryotic community composition. Our observations of a narrow range in the decrease of taxon-specific cells over time suggests grazing to be non-selective, but rather a function of the cell abundance and thus the encounter rate of a given taxon. In addition, prokaryotic community composition did not change substantially between visits at station M2, despite the high grazing activity. While a number of experimental studies carried out with freshwater communities demonstrate the influence of grazers on prokaryotic community composition (see review by Hahn and Höfle, 2001), experimental studies have revealed positive (Teira *et al.*, 2019) or no marked effects (Yokokawa and Nagata, 2005; Landa *et al.*, 2014; Baltar *et al.*, 2016) of the presence of grazers on marine prokaryotic diversity and composition. Our observations appear to be in line with these latter reports and suggest a minor influence of grazers on the temporal changes of the prokaryotic community composition in Kerguelen plateau waters.

4.5. Conclusions

Our observations from late Austral summer add another piece to the pictures obtained during early spring and summer and thereby extend our previous conclusions on the pronounced

effect of natural Fe fertilization on prokaryotic community composition to the post-bloom period. The accumulation of DOC, as a consequence of the high seasonal productivity in Kerguelen plateau waters, together with the potential prokaryote-diatom interactions contribute to the build-up of prokaryote bulk biomass and to their taxonomic composition. The capabilities in the access to different forms of Fe, key for the processing of organic matter, vary among prokaryotic groups (Debeljak *et al.*, 2019) and likely play an additional role in shaping microbial communities. Our results suggest that the most abundant prokaryotic taxa identified as specific to the productive Kerguelen plateau surface waters in late summer contribute to the transfer of organic matter to heterotrophic nanoflagellates (Christaki *et al.*, 2020) and potentially higher trophic levels.

5. References

595 Agogué, H., Lamy, D., Neal, P.R., Sogin, M.L., and Herndl, G.J. (2011) Water mass-specificity of bacterial communities in the North Atlantic revealed by massively parallel sequencing. Molecular Ecology 20: 258–274.

Armand, L.K., Cornet-Barthaux, V., Mosseri, J., and Quéguiner, B. (2008) Late summer diatom biomass and community structure on and around the naturally iron-fertilised 600 Kerguelen Plateau in the Southern Ocean. Deep Sea Research Part II: Topical Studies in Oceanography 55: 653–676.

Bachmann, J., Heimbach, T., Hassenrück, C., Kopprio, G.A., Iversen, M.H., Grossart, H.P., and Gärdes, A. (2018) Environmental Drivers of Free-Living vs. Particle-Attached Bacterial Community Composition in the Mauritania Upwelling System. Front Microbiol 9: 2836.

605 Baltar, F., Palovaara, J., Unrein, F., Catala, P., Horňák, K., Šimek, K., et al. (2016) Marine bacterial community structure resilience to changes in protist predation under phytoplankton bloom conditions. The ISME Journal 10: 568–581.

Barofsky, A., Vidoudez, C., and Pohnert, G. (2009) Metabolic profiling reveals growth stage variability in diatom exudates. Limnology and Oceanography: Methods 7: 382–390.

610 Belviso, S., Bopp, L., Mosseri, J., Tedetti, M., Garcia, N., Griffiths, B., et al. (2008) Effect of natural iron fertilisation on the distribution of DMS and DMSP in the Indian sector of the Southern Ocean. Deep Sea Research Part II: Topical Studies in Oceanography 55: 893–900.

Benner, R. and Strom, M. (1993) A critical evaluation of the analytical blank associated with DOC measurements by high-temperature catalytic oxidation. Marine Chemistry 41: 153–160.

Blain, S., Quéguiner, B., Armand, L., Belviso, S., Bombled, B., Bopp, L., et al. (2007) Effect of natural iron fertilization on carbon sequestration in the Southern Ocean. Nature 446: 1070–1074.

Blain, S., Rembauville, M., Crispi, O., and Obernosterer, I. (2020) Synchronized autonomous sampling reveals coupled pulses of biomass and export of morphologically different diatoms in the Southern Ocean. Limnology and Oceanography n/a:

Blazewicz, S.J., Barnard, R.L., Daly, R.A., and Firestone, M.K. (2013) Evaluating rRNA as an indicator of microbial activity in environmental communities: limitations and uses. The ISME Journal 7: 2061–2068.

Buchan, A., LeCleir, G.R., Gulvik, C.A., and González, J.M. (2014) Master recyclers: features and functions of bacteria associated with phytoplankton blooms. Nature Reviews Microbiology 12: 686–698.

Bunse, C. and Pinhassi, J. (2017) Marine Bacterioplankton Seasonal Succession Dynamics. Trends in Microbiology 25: 494–505.

Callahan, B.J., McMurdie, P.J., and Holmes, S.P. (2017) Exact sequence variants should replace operational taxonomic units in marker-gene data analysis. The ISME Journal 11: 2639–2643.

Callahan, B. J, McMurdie, P.J., Rosen, M.J., Han, A.W., Johnson, A.J.A., and Holmes, S.P. (2016a) DADA2: High resolution sample inference from Illumina amplicon data. Nat Methods 13: 581–583.

635 Callahan, B. J., Sankaran, K., Fukuyama, J.A., McMurdie, P.J., and Holmes, S.P. (2016b) Bioconductor Workflow for Microbiome Data Analysis: from raw reads to community analyses. F1000Res 5: 1492.

Christaki, U., Gueneugues, A., Liu, Y., Blain, S., Catala, P., Colombet, J., et al. (2020) Seasonal microbial food web dynamics in contrasting Southern Ocean productivity regimes.
640 Limnology and Oceanography n/a:

Christaki, U., Lefèvre, D., Georges, C., Colombet, J., Catala, P., Courties, C., et al. (2014) Microbial food web dynamics during spring phytoplankton blooms in the naturally iron-fertilized Kerguelen area (Southern Ocean). Biogeosciences 11: 6739–6753.

Christaki, U., Obernosterer, I., Van Wambeke, F., Veldhuis, M., Garcia, N., and Catala, P.
645 (2008) Microbial food web structure in a naturally iron-fertilized area in the Southern Ocean (Kerguelen Plateau). Deep Sea Research Part II: Topical Studies in Oceanography 55: 706–719.

Clarke, K.R. (1993) Non-parametric multivariate analyses of changes in community structure. Austral Ecol 18: 117–143.

650 Debeljak, P., Toulza, E., Beier, S., Blain, S., and Obernosterer, I. (2019) Microbial iron metabolism as revealed by gene expression profiles in contrasted Southern Ocean regimes. Environmental Microbiology 21: 2360–2374.

Ducklow, H.W., Hansell, D.A., and Morgan, J.A. (2007) Dissolved organic carbon and nitrogen in the Western Black Sea. Marine Chemistry 11.

Fuchs, B.M., Spring, S., Teeling, H., Quast, C., Wulf, J., Schattenhofer, M., et al. (2007) Characterization of a marine gammaproteobacterium capable of aerobic anoxygenic photosynthesis. PNAS 104: 2891–2896.

Georges, C., Monchy, S., Genitsaris, S., and Christaki, U. (2014) Protist community composition during early phytoplankton blooms in the naturally iron-fertilized Kerguelen area (Southern Ocean). Biogeosciences 11: 5847–5863.

Ghiglione, J.F., Mevel, G., Pujo-Pay, M., Mousseau, L., Lebaron, P., and Goutx, M. (2007) Diel and Seasonal Variations in Abundance, Activity, and Community Structure of Particle-Attached and Free-Living Bacteria in NW Mediterranean Sea. Microb Ecol 54: 217–231.

Gouy, M., Guindon, S., and Gascuel, O. (2010) SeaView Version 4: A Multiplatform Graphical User Interface for Sequence Alignment and Phylogenetic Tree Building. Mol Biol Evol 27: 221–224.

Guindon, S., Dufayard, J.-F., Lefort, V., Anisimova, M., Hordijk, W., and Gascuel, O. (2010) New Algorithms and Methods to Estimate Maximum-Likelihood Phylogenies: Assessing the Performance of PhyML 3.0. Systematic Biology 59: 307–321.

Hahn, M.W. and Höfle, M.G. (2001) Grazing of protozoa and its effect on populations of aquatic bacteria. FEMS Microbiology Ecology 35: 113–121.

Herlemann, D.P., Labrenz, M., Jürgens, K., Bertilsson, S., Waniek, J.J., and Andersson, A.F. (2011) Transitions in bacterial communities along the 2000 km salinity gradient of the Baltic Sea. The ISME Journal 5: 1571–1579.

675 Irion, S., Jardillier, L., Sassenhagen, I., and Christaki, U. (2020) Marked spatiotemporal variations in small phytoplankton structure in contrasted waters of the Southern Ocean (Kerguelen area). Limnology and Oceanography 65: 2835–2852.

Kappelmann, L., Krüger, K., Hehemann, J.-H., Harder, J., Markert, S., Unfried, F., et al. (2019) Polysaccharide utilization loci of North Sea Flavobacteriia as basis for using SusC/D-
680 protein expression for predicting major phytoplankton glycans. The ISME Journal 13: 76–91.

Katoh, K., Rozewicki, J., and Yamada, K.D. (2019) MAFFT online service: multiple sequence alignment, interactive sequence choice and visualization. Brief Bioinform 20: 1160–1166.

Kolde R. (2019). pheatmap: Pretty Heatmaps. R package version 1.0.12. https://CRAN.R-
685 project.org/package=pheatmap

Krüger, K., Chafee, M., Ben Francis, T., Glavina del Rio, T., Becher, D., Schweder, T., et al. (2019) In marine Bacteroidetes the bulk of glycan degradation during algae blooms is mediated by few clades using a restricted set of genes. The ISME Journal 13: 2800–2816.

Lafond, A., Leblanc, K., Legras, J., Cornet, V., and Quéguiner, B. (2020) The structure of
690 diatom communities constrains biogeochemical properties in surface waters of the Southern Ocean (Kerguelen Plateau). Journal of Marine Systems 212: 103458.

Landa, M., Blain, S., Christaki, U., Monchy, S., and Obernosterer, I. (2016) Shifts in bacterial community composition associated with increased carbon cycling in a mosaic of phytoplankton blooms. The ISME Journal 10: 39–50.

695 Landa, M., Cottrell, M.T., Kirchman, D.L., Kaiser, K., Medeiros, P.M., Tremblay, L., et al. (2014) Phylogenetic and structural response of heterotrophic bacteria to dissolved organic

matter of different chemical composition in a continuous culture study. Environmental Microbiology 16: 1668–1681.

Lasbleiz, M., Leblanc, K., Armand, L.K., Christaki, U., Georges, C., Obernosterer, I., and Quéguiner, B. (2016) Composition of diatom communities and their contribution to plankton biomass in the naturally iron-fertilized region of Kerguelen in the Southern Ocean. FEMS Microbiology Ecology 92:.

Legendre, P. and Gallagher, E.D. (2001) Ecologically meaningful transformations for ordination of species data. Oecologia 129: 271–280.

Legendre, P. and Legendre, L. (2012) Canonical analysis. In Developments in Environmental Modelling. Elsevier, pp. 625–710.

Liu, Y., Blain, S., Crispi, O., Rembauville, M., and Obernosterer, I. (2020) Seasonal dynamics of prokaryotes and their associations with diatoms in the Southern Ocean as revealed by an autonomous sampler. Environmental Microbiology 22: 3968–3984.

Liu, Y., Debeljak, P., Rembauville, M., Blain, S., and Obernosterer, I. (2019) Diatoms shape the biogeography of heterotrophic prokaryotes in early spring in the Southern Ocean. Environmental Microbiology 21: 1452–1465.

McMurdie, P.J. and Holmes, S. (2013) phyloseq: An R Package for Reproducible Interactive Analysis and Graphics of Microbiome Census Data. PLOS ONE 8: e61217.

Mitulla, M., Dinasquet, J., Guillemette, R., Simon, M., Azam, F., and Wietz, M. (2016) Response of bacterial communities from California coastal waters to alginate particles and an alginolytic Alteromonas macleodii strain. Environmental Microbiology 18: 4369–4377.

Myklestad, S., Holm-Hansen, O., Vårum, K.M., and Volcani, B.E. (1989) Rate of release of extracellular amino acids and carbohydrates from the marine diatom Chaetoceros affinis. Journal of Plankton Research 11: 763–773.

Nowinski, B., Motard□Côté, J., Landa, M., Preston, C.M., Scholin, C.A., Birch, J.M., et al. (2019) Microdiversity and temporal dynamics of marine bacterial dimethylsulfoniopropionate genes. Environmental Microbiology 21: 1687–1701.

Obernosterer, I., Catala, P., Lebaron, P., and West, N.J. (2011) Distinct bacterial groups contribute to carbon cycling during a naturally iron fertilized phytoplankton bloom in the Southern Ocean. Limnology and Oceanography 56: 2391–2401.

Obernosterer, I., Fourquez, M., and Blain, S. (2015) Fe and C co-limitation of heterotrophic bacteria in the naturally fertilized region off the Kerguelen Islands. Biogeosciences 12: 1983–1992.

Oksanen, J., Blanchet, F.G., Kindt, R., Legendre, P., Minchin, P.R., O'Hara, R.B., et al. (2019) vegan: community ecology package. R Package Version 2.5-6. https://CRAN.R-project.org/package=vegan

Ortega-Retuerta, E., Joux, F., Jeffrey, W.H., and Ghiglione, J.F. (2013) Spatial variability of particle-attached and free-living bacterial diversity in surface waters from the Mackenzie River to the Beaufort Sea (Canadian Arctic). Biogeosciences 10: 2747–2759.

Parada, A.E., Needham, D.M., and Fuhrman, J.A. (2016) Every base matters: assessing small subunit rRNA primers for marine microbiomes with mock communities, time series and global field samples. Environmental Microbiology 18: 1403–1414.

Pauthenet, E., Roquet, F., Madec, G., Guinet, C., Hindell, M., McMahon, C.R., et al. (2018) Seasonal Meandering of the Polar Front Upstream of the Kerguelen Plateau. Geophysical Research Letters 45: 9774–9781.

Quast, C., Pruesse, E., Yilmaz, P., Gerken, J., Schweer, T., Yarza, P., et al. (2013) The SILVA ribosomal RNA gene database project: improved data processing and web-based tools. Nucleic Acids Res 41: D590–D596.

R Core Team (2019). R: A language and environment for statistical computing. R Foundation for Statistical Computing, Vienna, Austria. URL https://www.R-project.org/

Ras, J., Claustre, H., and Uitz, J. (2008) Spatial variability of phytoplankton pigment distributions in the Subtropical South Pacific Ocean: comparison between in situ and predicted data. 17.

Rieck, A., Herlemann, D.P.R., Jürgens, K., and Grossart, H.-P. (2015) Particle-Associated Differ from Free-Living Bacteria in Surface Waters of the Baltic Sea. Front Microbiol 6:.

Sassenhagen, I., Irion, S., Jardillier, L., Moreira, D., and Christaki, U. (2020) Protist Interactions and Community Structure During Early Autumn in the Kerguelen Region (Southern Ocean). Protist 171: 125709.

Schoemann, V., Becquevort, S., Stefels, J., Rousseau, V., and Lancelot, C. (2005) Phaeocystis blooms in the global ocean and their controlling mechanisms: a review. Journal of Sea Research 53: 43–66.

Steiner, P.A., Sintes, E., Simó, R., Corte, D.D., Pfannkuchen, D.M., Ivančić, I., et al. (2019) Seasonal dynamics of marine snow-associated and free-living demethylating bacterial

communities in the coastal northern Adriatic Sea. Environmental Microbiology Reports 11: 699–707.

Steinberg, D.K. and Landry, M.R. (2017) Zooplankton and the Ocean Carbon Cycle. Annu Rev Mar Sci 9: 413–444.

Stoddard, S.F., Smith, B.J., Hein, R., Roller, B.R.K., and Schmidt, T.M. (2015) rrnDB: improved tools for interpreting rRNA gene abundance in bacteria and archaea and a new foundation for future development. Nucleic Acids Res 43: D593–D598.

Sun, Y., P. Debeljak and I. Obernosterer (in press) Microbial iron and carbon metabolism as revealed by functional diversity in the Southern Ocean. ISMEJ DOI:10.1038/s41396-021-00973-3

Teeling, H., Fuchs, B.M., Becher, D., Klockow, C., Gardebrecht, A., Bennke, C.M., et al. (2012) Substrate-Controlled Succession of Marine Bacterioplankton Populations Induced by a Phytoplankton Bloom. Science 336: 608–611.

Teira, E., Logares, R., Gutiérrez□Barral, A., Ferrera, I., Varela, M.M., Morán, X.A.G., and Gasol, J.M. (2019) Impact of grazing, resource availability and light on prokaryotic growth and diversity in the oligotrophic surface global ocean. Environmental Microbiology 21: 1482–1496.

West, N.J., Obernosterer, I., Zemb, O., and Lebaron, P. (2008) Major differences of bacterial diversity and activity inside and outside of a natural iron-fertilized phytoplankton bloom in the Southern Ocean. Environmental Microbiology 10: 738–756.

Xing, P., Hahnke, R.L., Unfried, F., Markert, S., Huang, S., Barbeyron, T., et al. (2015) Niches of two polysaccharide-degrading Polaribacter isolates from the North Sea during a spring diatom bloom. The ISME Journal 9: 1410–1422.

Yokokawa, T. and Nagata, T. (2005) Growth and Grazing Mortality Rates of Phylogenetic Groups of Bacterioplankton in Coastal Marine Environments. Appl Environ Microbiol 71: 6799–6807.

Zhang, R., Liu, B., Lau, S.C.K., Ki, J.-S., and Qian, P.-Y. (2007) Particle-attached and free-living bacterial communities in a contrasting marine environment: Victoria Harbor, Hong Kong. FEMS Microbiology Ecology 61: 496–508.

Zhang, Y., Jing, H., and Peng, X. (2020) Vertical shifts of particle-attached and free-living prokaryotes in the water column above the cold seeps of the South China Sea. Marine Pollution Bulletin 156: 111230.

Figure Legends

Figure 1. Map of the MOBYDICK station locations. Surface chlorophyll concentrations are from Global Ocean Satellite Observations (Copernicus-GlobColour). Reprocessed data are provided by Copernicus Marine Service. Chlorophyll concentrations are the monthly mean for March 2018 at a resolution of 4 km. The black lines denote 1000 m bathymetry.

Figure 2. Vertical profiles of Chl *a*, DOC and prokaryotic abundance at the on-plateau station M2 and the off-plateau stations M3 and M4. Chl*a* and prokaryotic abundances are shown for each visit, DOC concentration is given as the mean of the repeated visits. Data for station M1 are shown in Fig. S3.

Figure 3. Non-Metric Multidimensional Scaling (NMDS) of total (DNA) prokaryotic communities in the (a) free-living and (b) particle-attached fraction from all depth layers based on Bray-Curtis Dissimilarity. Sample depths are indicated by color, sampling sites by symbol and the number of visit is indicated with a number next to the respective symbol (see Table 1 for more information about sampling scheme.)

Figure 4. Relative abundance of total (DNA) free-living (FL) and particle-attached (PA) taxa grouped at order level in surface waters (10 m). For stations M2, M3 and M4 the relative abundances of the first visit are shown.

Figure 5. Relative abundance of ASVs that contribute significantly ($p<0.05$) to the dissimilarity between stations M2 and M3 (SIMPER analysis) at 10m. Asterisk highlight significant differences for a given ASV between sites, in either the free-living or particle-attached fractions, for the total (DNA) or potentially active (RNA) communities. Only the ASVs with relative abundance >5% in at least one of the samples are shown. Note that the

ASVs that contribute to the difference among sites are not always the same for the total and the active communities

Figure 6. Changes in the absolute abundance of dominant taxa (DNA, free-living fraction) between the first and the second (M2_3) and the first and the third (M2_3) visit at station M2 at 10 m. Deviations are given as percent; positive and negative values indicate an increase and a decrease, respectively, in abundance over the repeated visits at station M2. The deviation was calculated based on a formula published in Agogué *et al.* (2011).

Sequencing data. Demultiplexed sequence files are available in NCBI under accession number PRJNA679029.

Acknowledgments

We thank B. Quéguiner, the PI of the MOBYDICK project, for providing us the opportunity to participate to this cruise, and the captain and crew of the *R/V* Marion Dufresne for their enthusiasm and support aboard during the MOBYDICK– THEMISTO cruise (https://doi.org/10.17600/18000403). This work was supported by the French oceanographic fleet ("Flotte océanographique française"), the French ANR ("Agence Nationale de la Recherche", AAPG 2017 program, MOBYDICK Project number : ANR-17-CE01-0013), and the French Research program of INSU-CNRS LEFE/CYBER ("Les enveloppes fluides et l'environnement" – "Cycles biogéochimiques, environnement et ressources"). We thank P. Catala for flow cytometry analyses. We are grateful to A. Lafond and J. Legras for sharing with us the diatom species abundances obtained by microscopic observations. We thank the GenoToul Bioinformatics platform (http://bioinfo.genotoul.fr/) for providing computing resources. Y.L. was supported by the China Scholarship Council (CSC; No. 201606330072). Three reviewers provided constructive comments that helped improve a previous version of the manuscript.

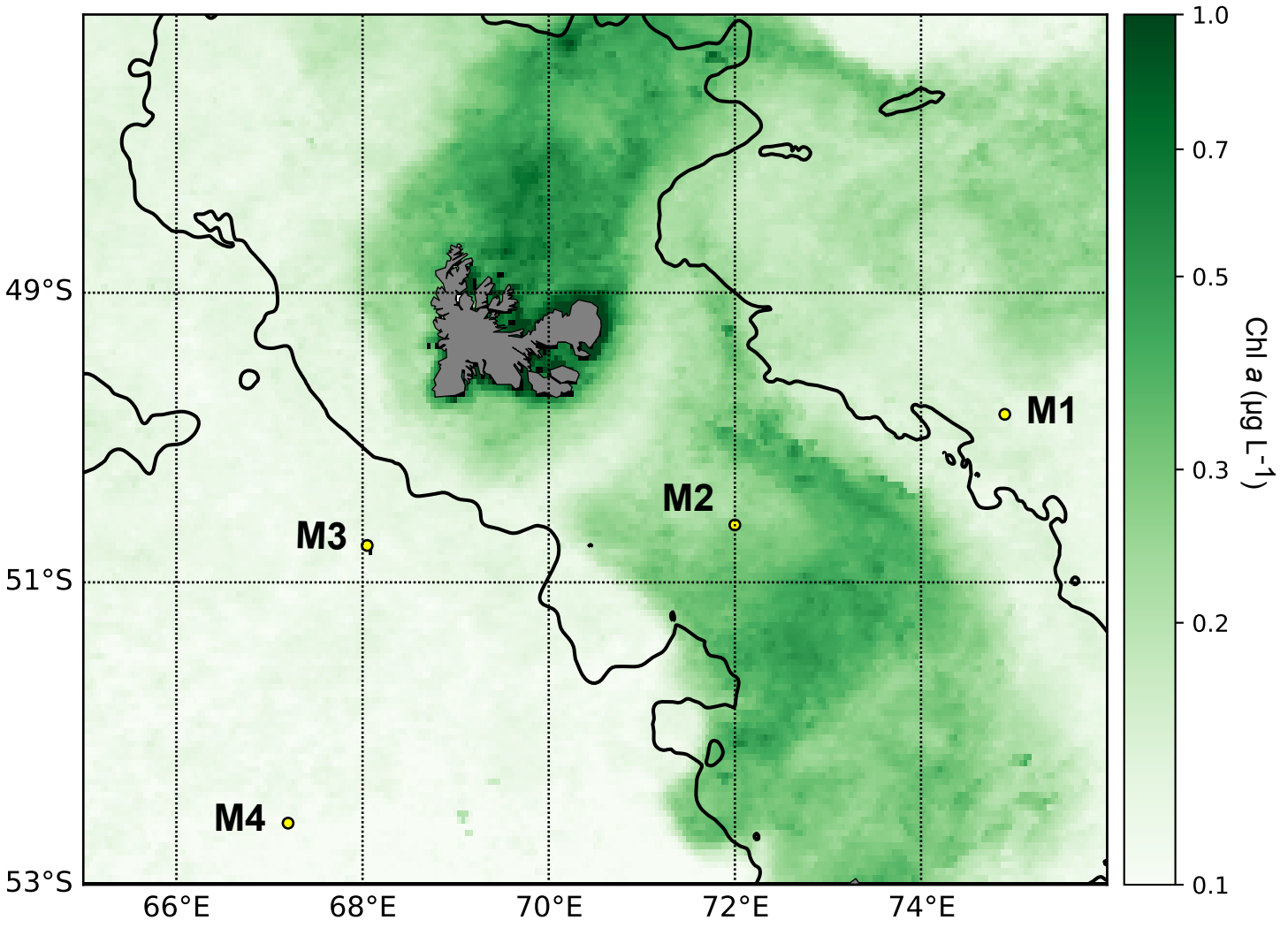
49°S
51°S
53°S
66°E
68°E
70°E
72°E
74°E
M1
M2
M3
M4
1.0
0.7
0.5
0.3
0.2
0.1
Chl a (µg L-1)

Fig. 1

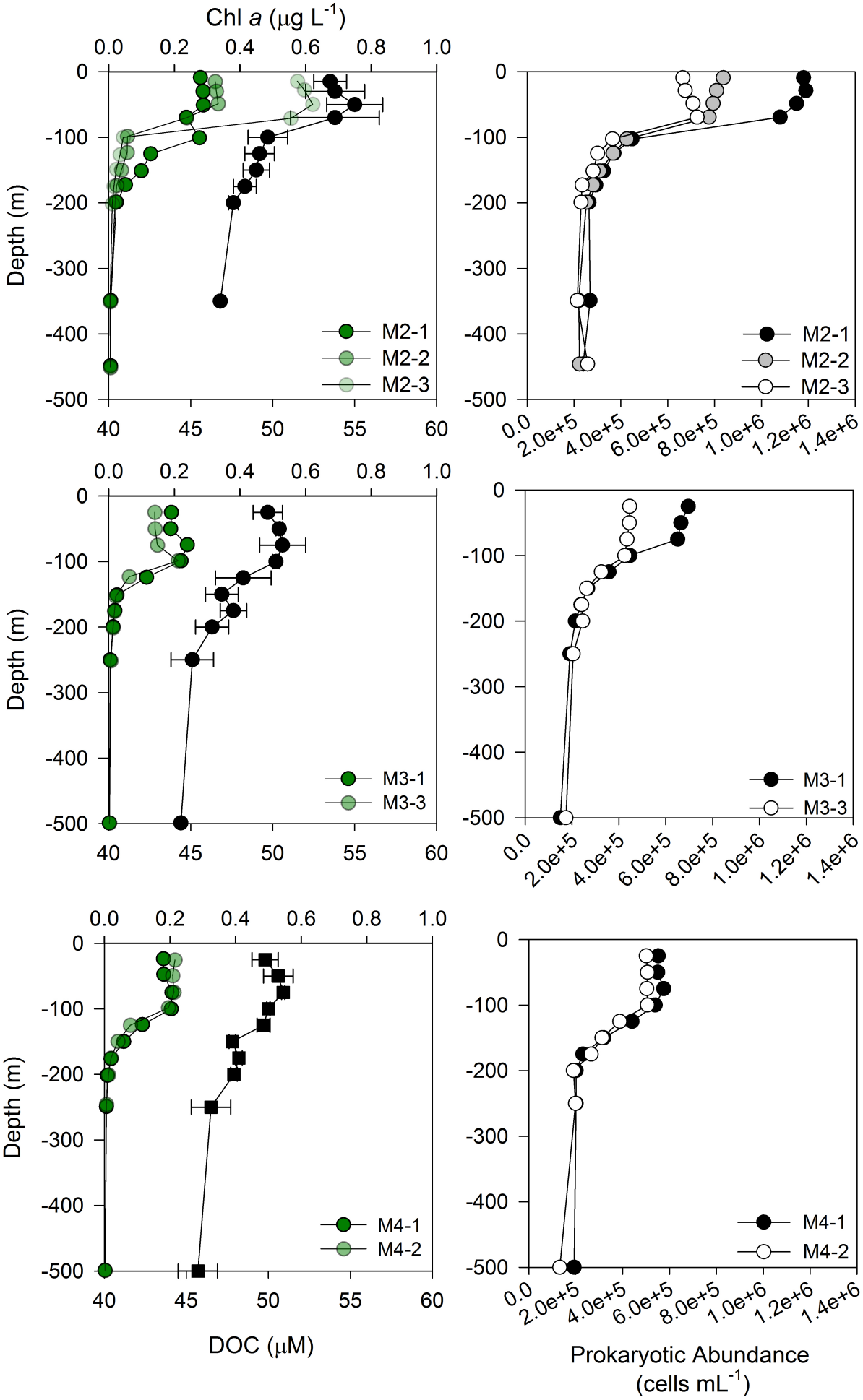
Chl a (μg L-1)
Depth (m)
M2-1
M2-2
M2-3
M3-1
M3-3
M4-1
M4-2
DOC (μM)
Prokaryotic Abundance
(cells mL-1)

Fig. 2

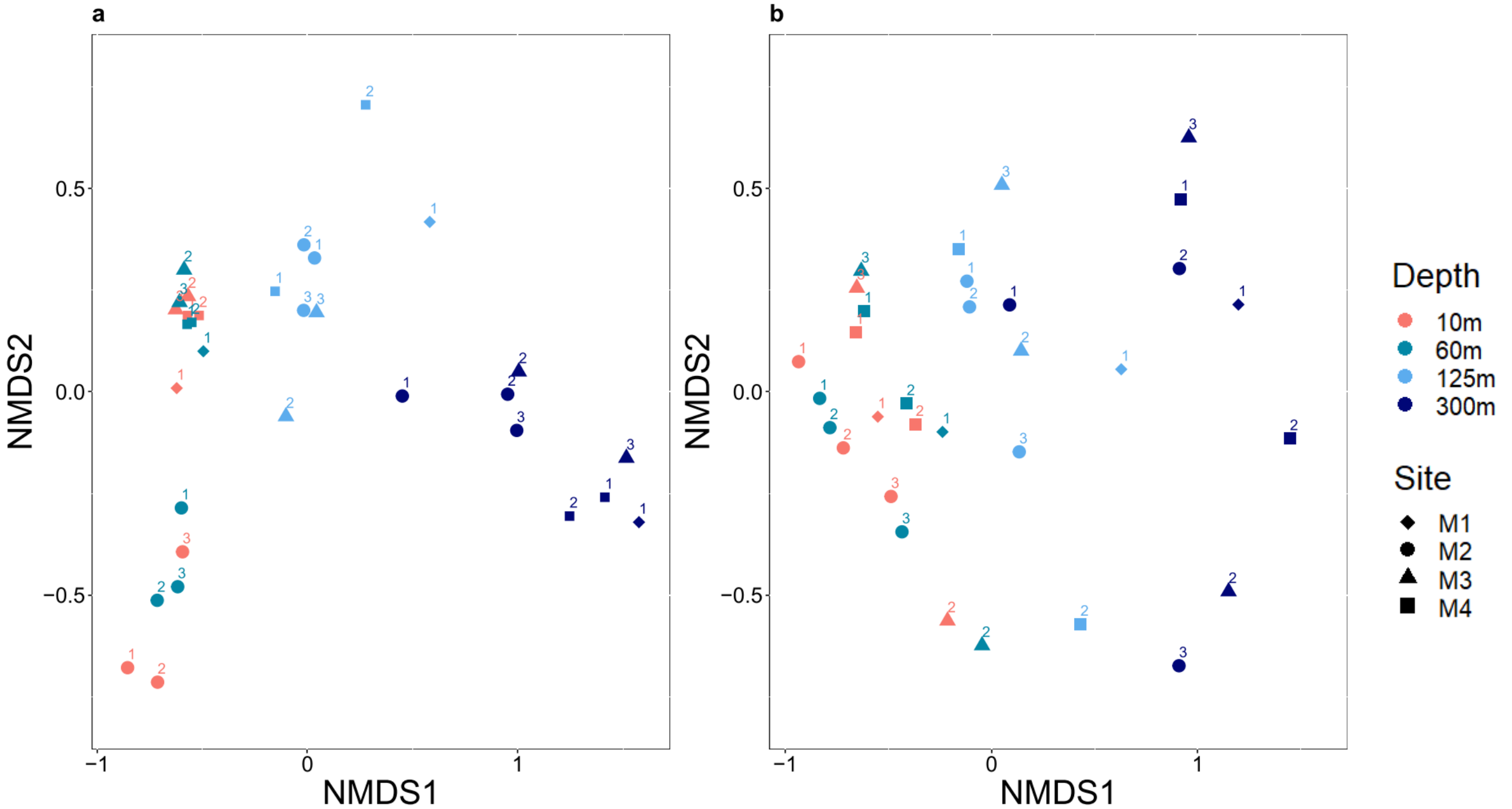
a
b
NMDS1
NMDS2
0.5
0.0
−0.5
−1
0
1
Depth
10m
60m
125m
300m
Site
M1
M2
M3
M4

Fig. 3

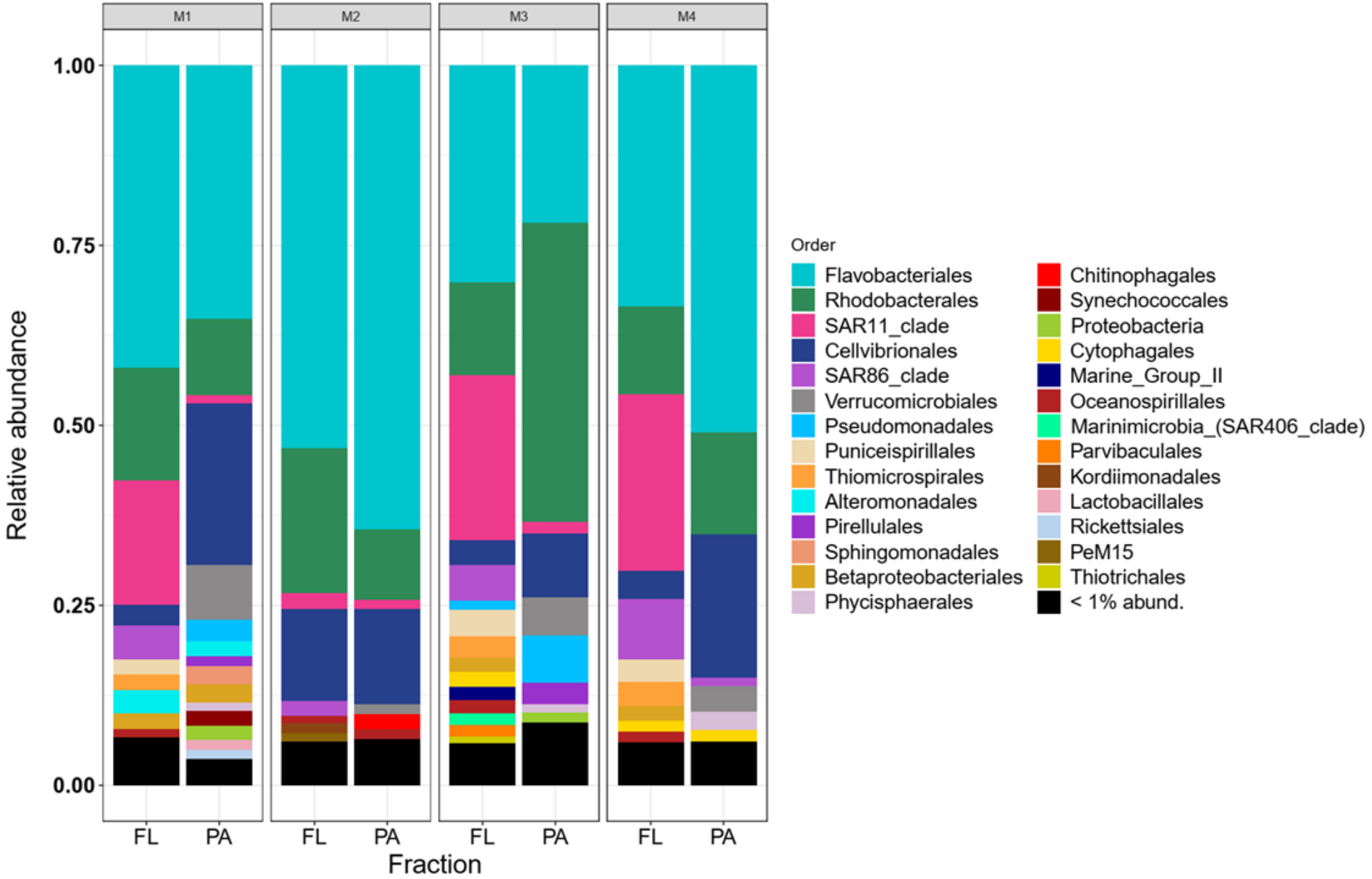
M1
M2
M3
M4
1.00
0.75
0.50
0.25
0.00
Relative abundance
FL
PA
Fraction
Order
Flavobacteriales
Rhodobacterales
SAR11_clade
Cellvibrionales
SAR86_clade
Verrucomicrobiales
Pseudomonadales
Puniceispirillales
Thiomicrospirales
Alteromonadales
Pirellulales
Sphingomonadales
Betaproteobacteriales
Phycisphaerales
Chitinophagales
Synechococcales
Proteobacteria
Cytophagales
Marine_Group_II
Oceanospirillales
Marinimicrobia_(SAR406_clade)
Parvibaculales
Kordiimonadales
Lactobacillales
Rickettsiales
PeM15
Thiotrichales
< 1% abund.

Fig. 4

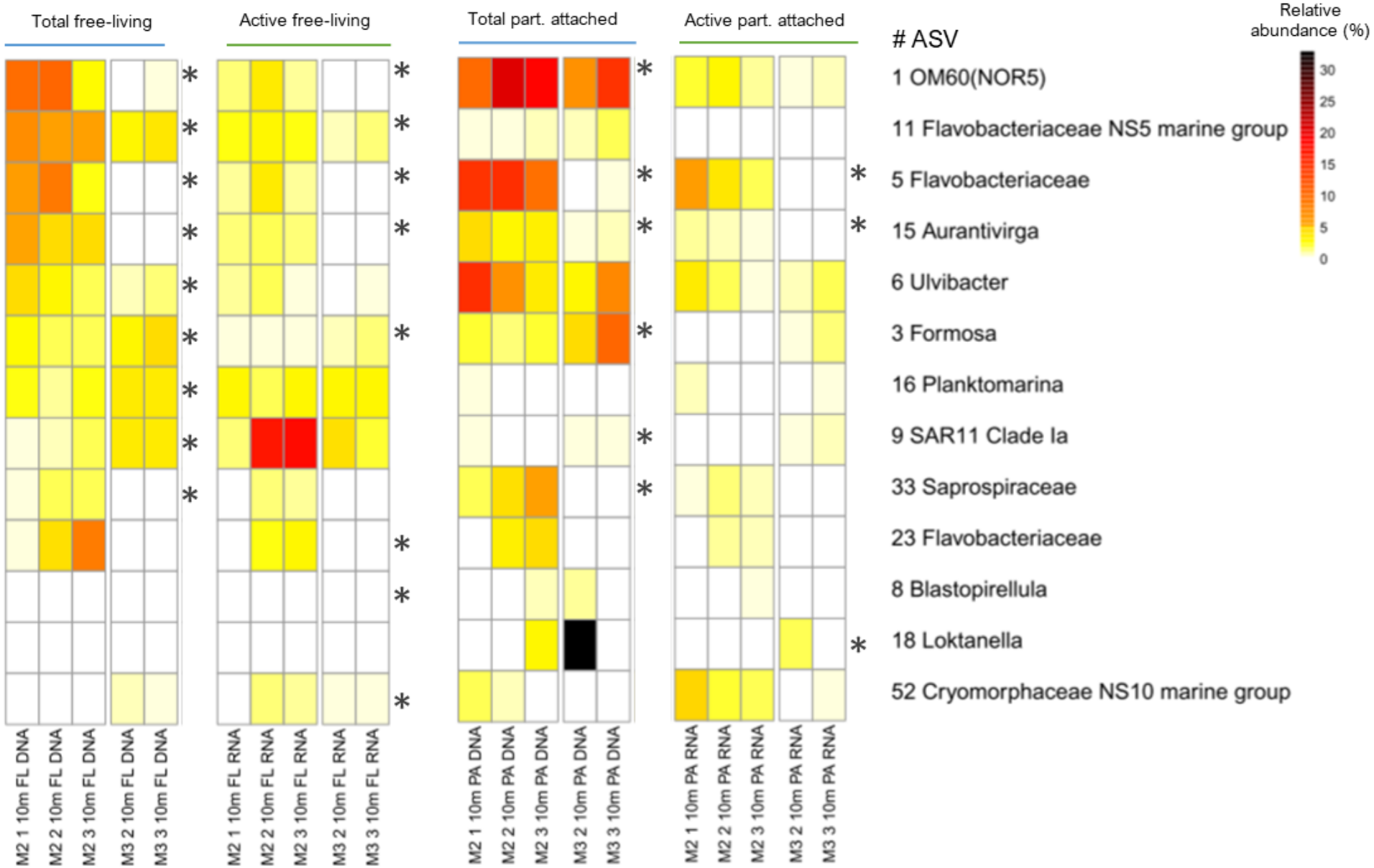
Total free-living
Active free-living
Total part. attached
Active part. attached
ASV
Relative abundance (%)
30
25
20
15
10
5
0
1 OM60(NOR5)
11 Flavobacteriaceae NS5 marine group
5 Flavobacteriaceae
15 Aurantivirga
6 Ulvibacter
3 Formosa
16 Planktomarina
9 SAR11 Clade Ia
33 Saprospiraceae
23 Flavobacteriaceae
8 Blastopirellula
18 Loktanella
52 Cryomorphaceae NS10 marine group
M2 1 10m FL DNA
M2 2 10m FL DNA
M2 3 10m FL DNA
M3 2 10m FL DNA
M3 3 10m FL DNA
M2 1 10m FL RNA
M2 2 10m FL RNA
M2 3 10m FL RNA
M3 2 10m FL RNA
M3 3 10m FL RNA
M2 1 10m PA DNA
M2 2 10m PA DNA
M2 3 10m PA DNA
M3 2 10m PA DNA
M3 3 10m PA DNA
M2 1 10m PA RNA
M2 2 10m PA RNA
M2 3 10m PA RNA
M3 2 10m PA RNA
M3 3 10m PA RNA

Fig. 5

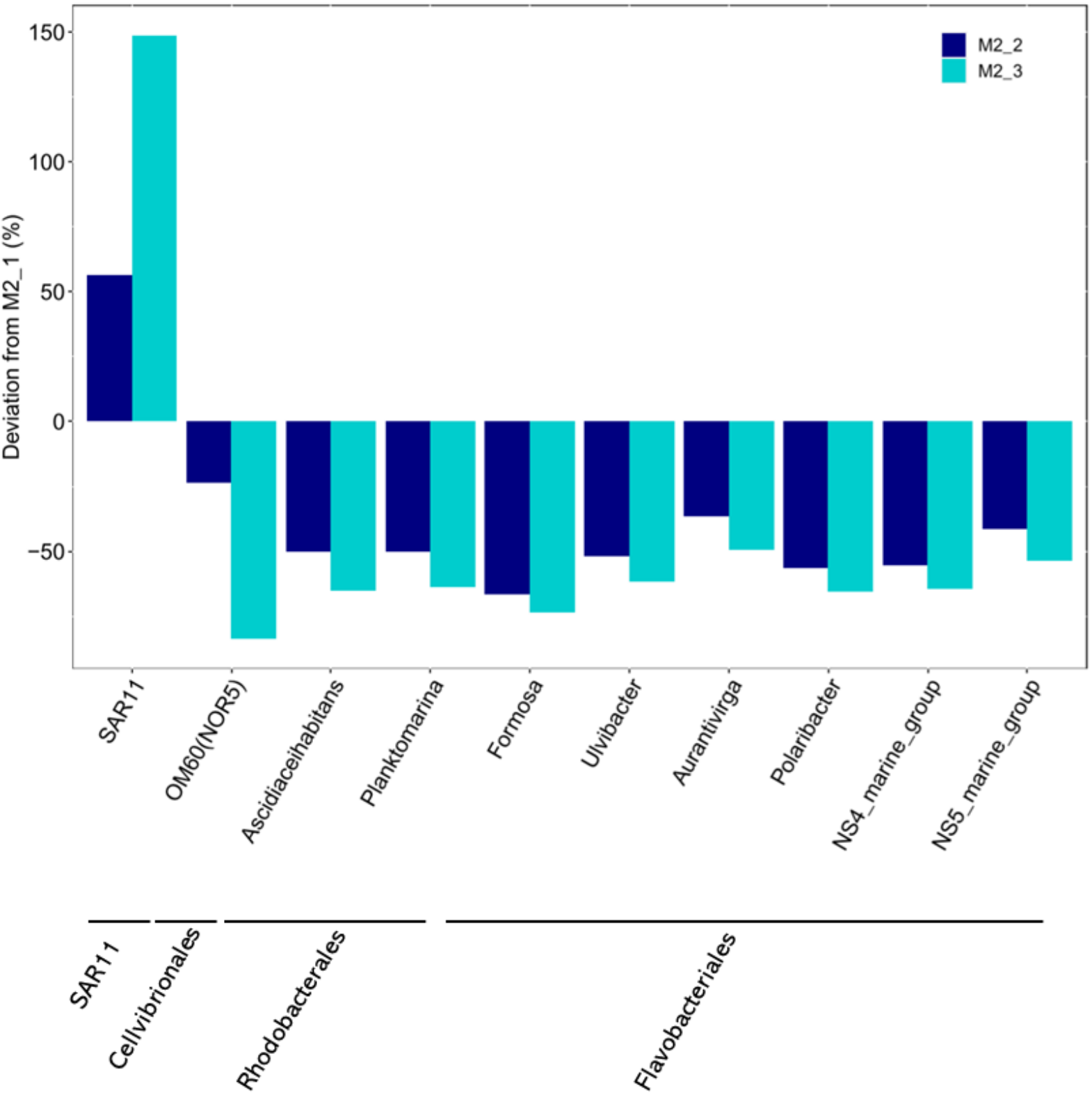
150
100
50
0
−50
Deviation from M2_1 (%)
M2_2
M2_3
SAR11
OM60(NOR5)
Ascidiaceihabitans
Planktomarina
Formosa
Ulvibacter
Aurantivirga
Polaribacter
NS4_marine_group
NS5_marine_group
SAR11
Cellvibrionales
Rhodobacterales
Flavobacteriales

Fig. 6

Table 1. Brief description of the study sites. The wind-mixed surface layer (Z_{ML}) is based on a difference in sigma of 0.02 to the surface value. Mean±SD of the Z_{ML} are given

Station	Lat/Long	Depth (m)	Date	Z_{ML} (m)	Temp Z_{ML} (°C)	Chl *a* Z_{ML} (μg L^{-1})	DOC Z_{ML} (μM)
On plateau							
M2-1	50.61°S 72.00°E	527	26 Feb	62	5.1±0.06	0.27±0.02	52.8±0.5
M2-2			06 Mar	61	5.2±0.00	0.30±0.04	55.7±1.1
M2-3			16 Mar	68	5.1±0.07	0.58±0.02	53.8±1.1
Off plateau							
M1	49.84°S 74.90°E	2723	09 March	27	4.9±0.10	0.35±0.04	50.3*
M3-1	50.68°S	1700	04 Mar	65	5.6±0.00	0.20±0.02	50.3±0.1
M3-3	68.05°E		19 Mar	79	5.3±0.02	0.14±0.00	50.4±1.3
M4-1	52.60°S	4300	01 Mar	49	4.5±0.06	0.18±0.01	49.6±0.5
M4-2	67.19°E		12 Mar	87	4.5±0.00	0.21±0.00	50.8±0.4

*only one data point in the Z_{ML} available

Station M3-2 was not sampled for the parameters considered in the present study

Table 2. Prokaryotic diversity as illustrated by the Shannon Index. Results for the first visit to the off-plateau stations are shown. A full description of the diversity indices is provided in Table S1. NA – Not Available

	Total (DNA)		Active (RNA)	
Depth (m)	Free-living	Particle-attached	Free-living	Particle-attached
		On Plateau		
Station M2-1				
10	4.05	3.67	6.04	5.79
50	4.52	3.59	NA	5.95
100	4.97	3.96	6.37	6.19
300	5.32	4.61	5.97	6.45
Station M2-2				
10	4.20	3.69	4.59	5.89
60	4.32	3.41	6.04	4.51
125	4.92	4.12	5.21	5.03
300	5.39	5.69	5.99	6.34
Station M2-3				
10	4.56	3.65	4.79	6.37
60	4.38	3.54	4.94	5.85
125	5.04	3.80	6.56	6.22
300	5.37	3.99	6.66	4.90
		Off plateau		
Station M1				
10	4.63	4.01	4.39	6.22
60	4.91	3.91	6.26	6.05
125	5.02	5.07	6.55	6.66
300	5.17	6.01	5.64	6.42
Station M3-1				
10	5.01	3.52	6.15	6.04
60	5.12	3.29	6.44	5.91
125	5.00	3.66	4.86	6.20
300	5.57	4.77	6.37	5.76
Station M4-1				
10	4.78	3.72	5.65	6.04
60	4.76	3.88	5.94	6.21
125	5.10	4.40	6.52	6.56
300	5.45	5.65	6.01	6.29

Supplementary Material

for the manuscript

Prokaryotic diversity and activity in contrasting productivity regimes in late summer in the Kerguelen region (Southern Ocean)

Alejandra Elisa Hernandez-Magana [1,2]*, Yan Liu [1, 3]*, Pavla Debeljak[1,4†], Olivier Crispi[1], Barbara Marie[1], Coco Koedooder[1‡], Ingrid Obernosterer[1#]

This file contains
10 Suppl. Figures
4 Suppl. Tables

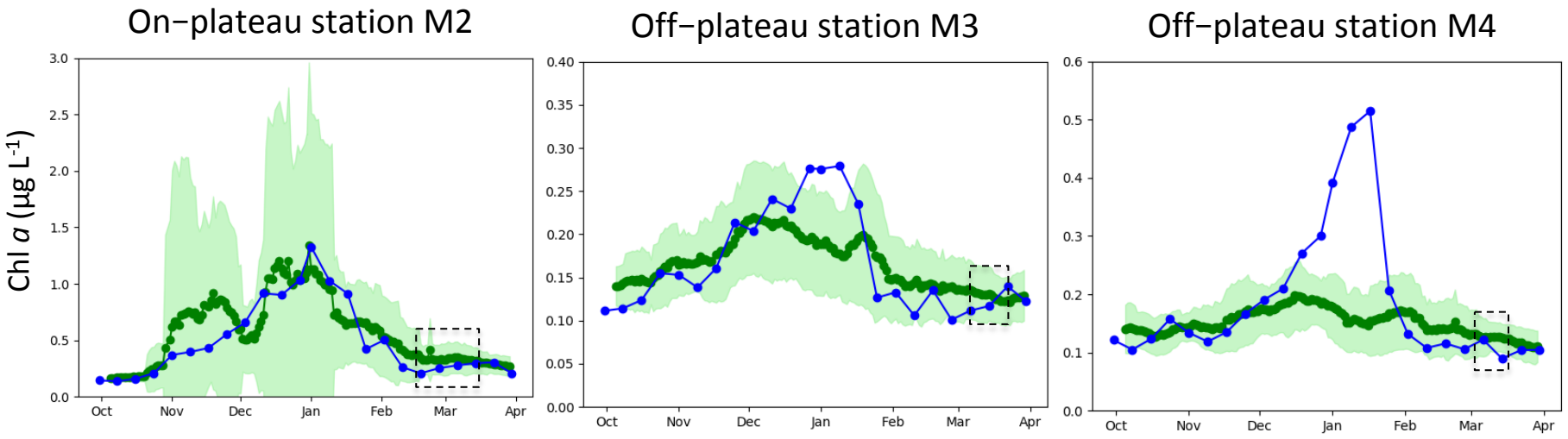
On−plateau station M2
Off−plateau station M3
Off−plateau station M4
Chl a (µg L-1)
3.0
2.5
2.0
1.5
1.0
0.5
0.0
0.40
0.35
0.30
0.25
0.20
0.15
0.10
0.05
0.00
0.6
0.5
0.4
0.3
0.2
0.1
0.0
Oct
Nov
Dec
Jan
Feb
Mar
Apr

Fig. S1

Fig. S2

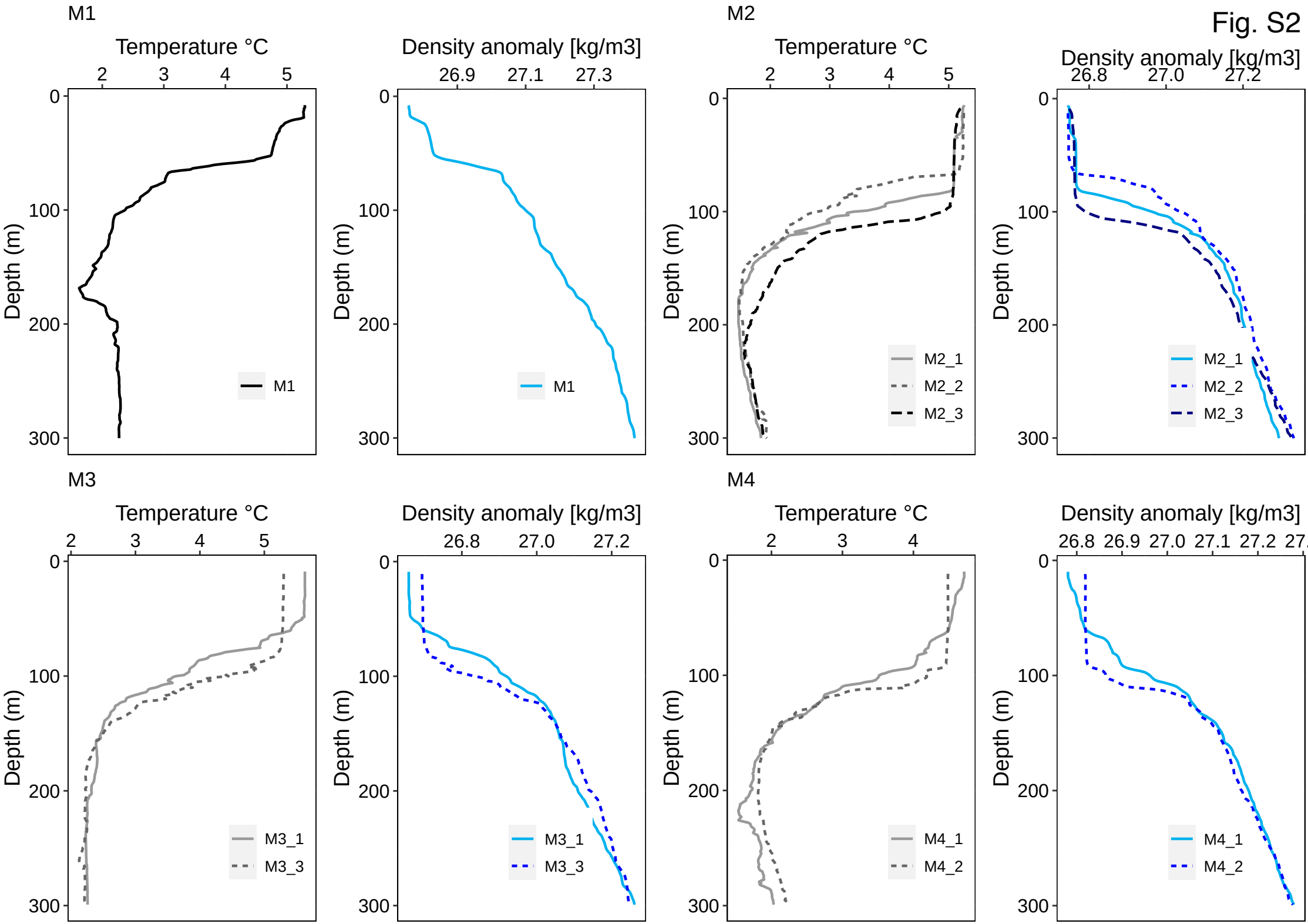
M1
Temperature °C
Density anomaly [kg/m3]
M2
Temperature °C
Density anomaly [kg/m3]
M3
Temperature °C
Density anomaly [kg/m3]
M4
Temperature °C
Density anomaly [kg/m3]
Depth (m)
M1
M2_1
M2_2
M2_3
M3_1
M3_3
M4_1
M4_2

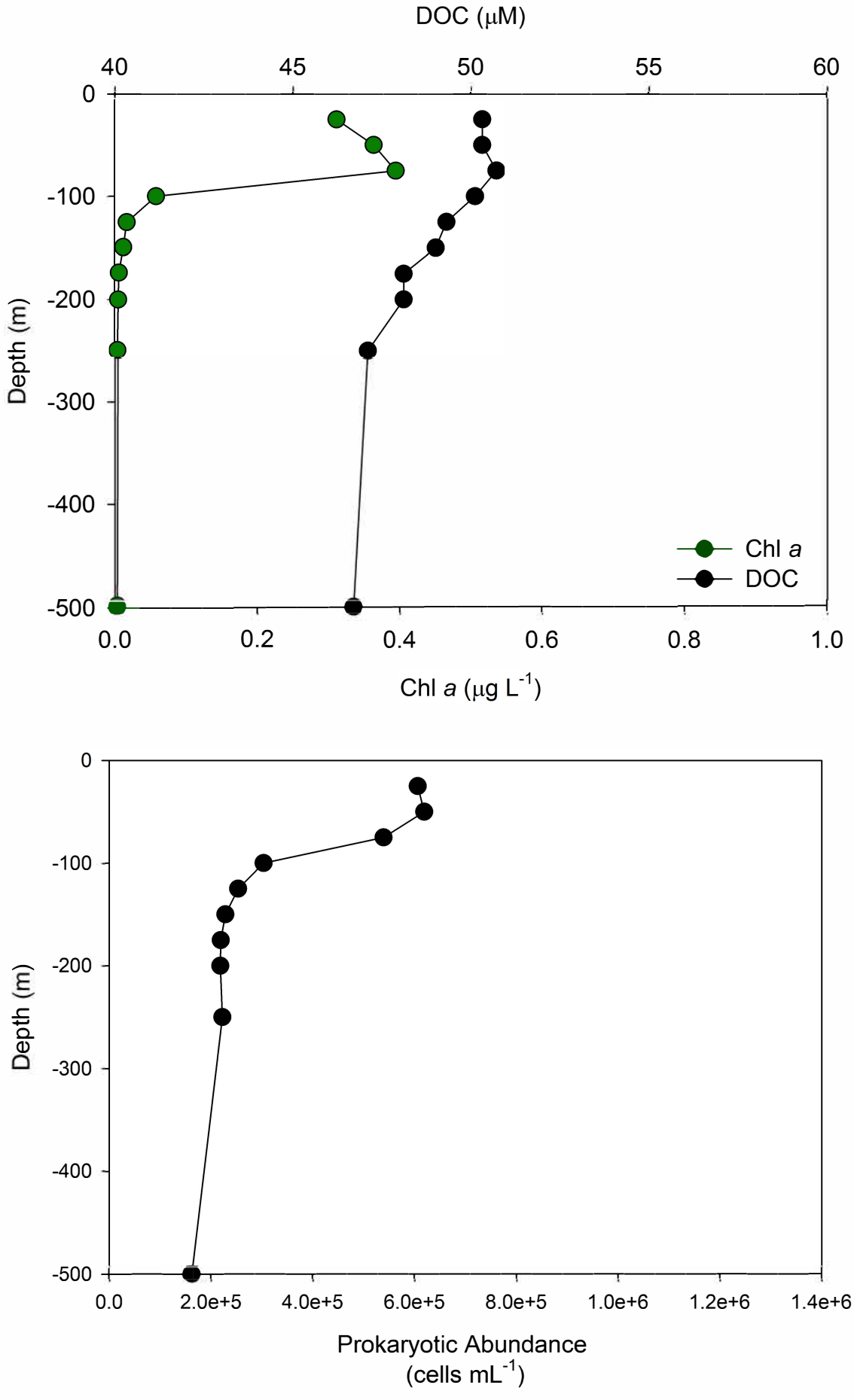
DOC (μM)
40
45
50
55
60
0
-100
-200
-300
-400
-500
Depth (m)
Chl a
DOC
0.0
0.2
0.4
0.6
0.8
1.0
Chl a (μg L-1)
0
-100
-200
-300
-400
-500
Depth (m)
0.0
2.0e+5
4.0e+5
6.0e+5
8.0e+5
1.0e+6
1.2e+6
1.4e+6
Prokaryotic Abundance
(cells mL-1)

Fig. S3

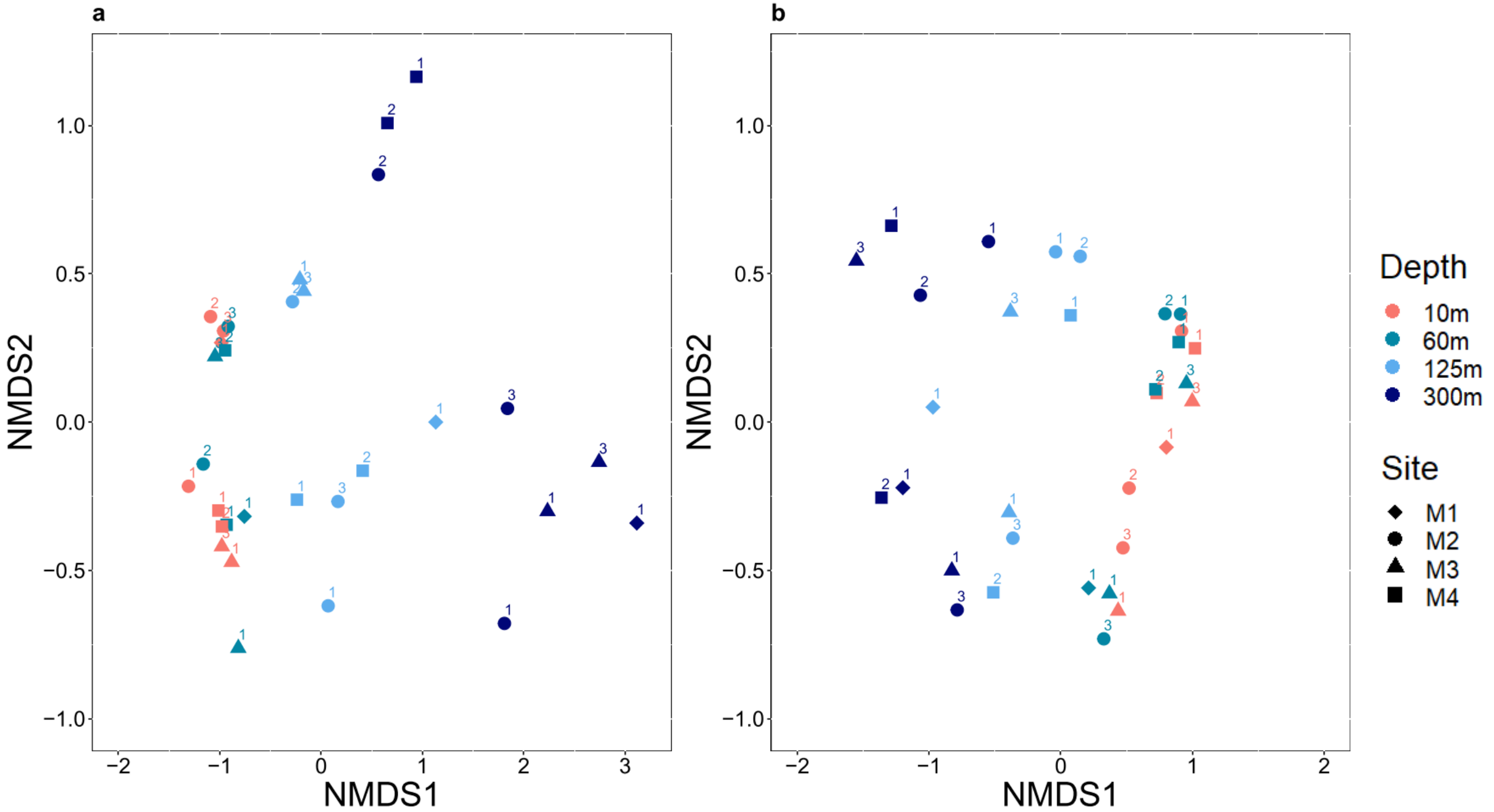

Fig. S4

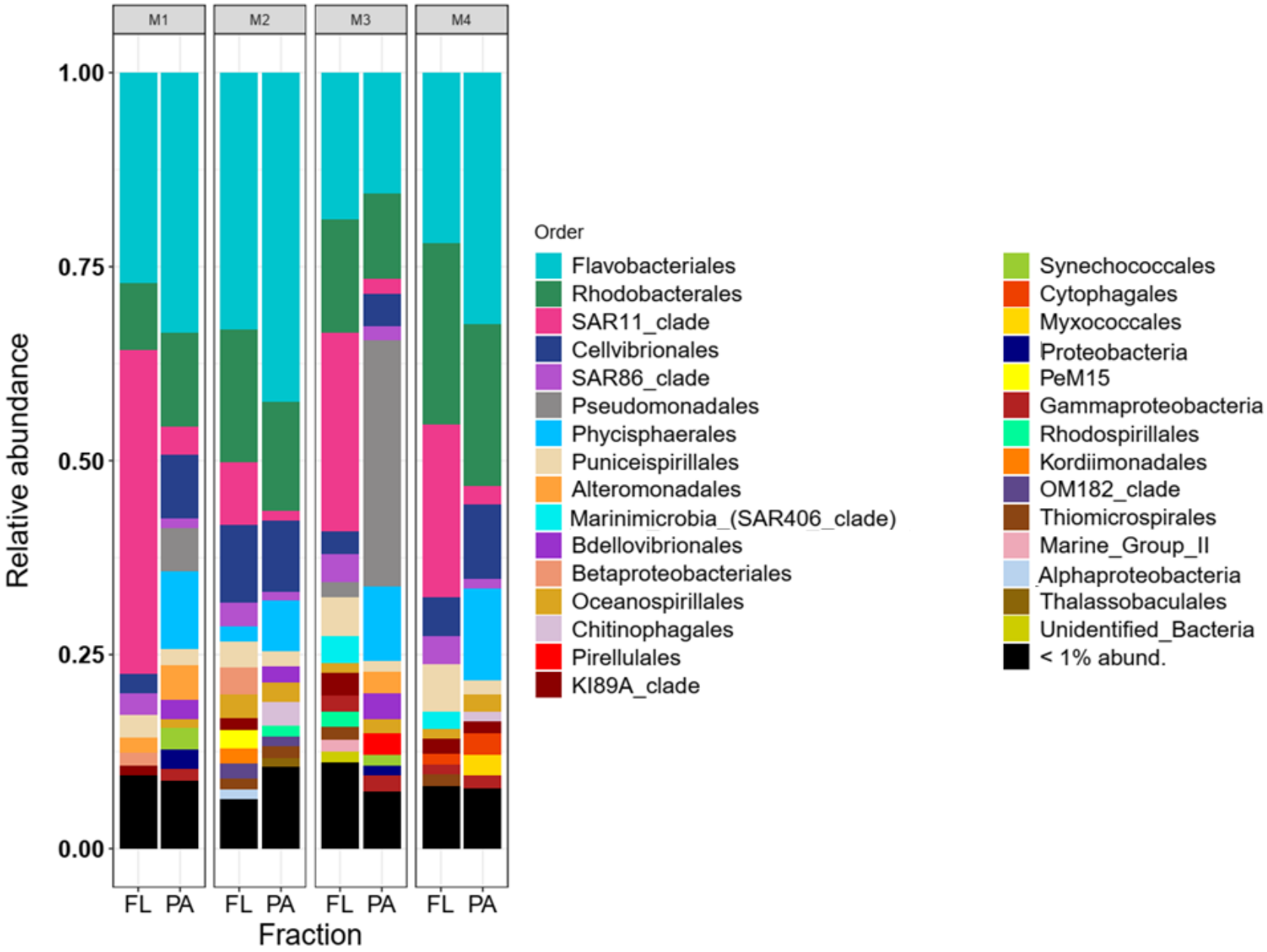
M1
M2
M3
M4
1.00
0.75
0.50
0.25
0.00
Relative abundance
FL
PA
Fraction
Order
Flavobacteriales
Rhodobacterales
SAR11_clade
Cellvibrionales
SAR86_clade
Pseudomonadales
Phycisphaerales
Puniceispirillales
Alteromonadales
Marinimicrobia_(SAR406_clade)
Bdellovibrionales
Betaproteobacteriales
Oceanospirillales
Chitinophagales
Pirellulales
KI89A_clade
Synechococcales
Cytophagales
Myxococcales
Proteobacteria
PeM15
Gammaproteobacteria
Rhodospirillales
Kordiimonadales
OM182_clade
Thiomicrospirales
Marine_Group_II
Alphaproteobacteria
Thalassobaculales
Unidentified_Bacteria
< 1% abund.

Fig. S5

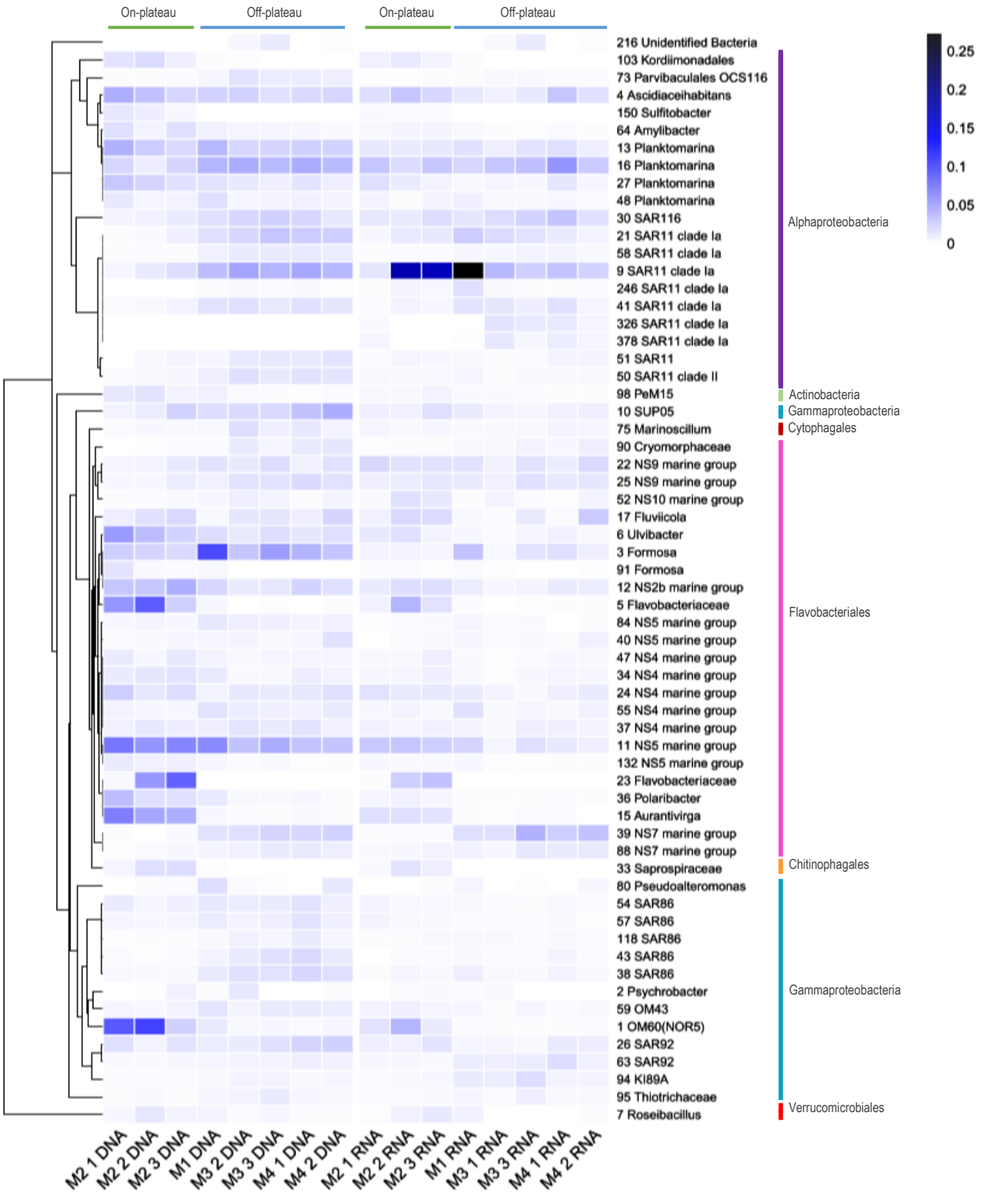
On-plateau
Off-plateau
On-plateau
Off-plateau
0.25
0.2
0.15
0.1
0.05
0
216 Unidentified Bacteria
103 Kordiimonadales
73 Parvibaculales OCS116
4 Ascidiaceihabitans
150 Sulfitobacter
64 Amylibacter
13 Planktomarina
16 Planktomarina
27 Planktomarina
48 Planktomarina
30 SAR116
21 SAR11 clade Ia
58 SAR11 clade Ia
9 SAR11 clade Ia
246 SAR11 clade Ia
41 SAR11 clade Ia
326 SAR11 clade Ia
378 SAR11 clade Ia
51 SAR11
50 SAR11 clade II
98 PeM15
10 SUP05
75 Marinoscillum
90 Cryomorphaceae
22 NS9 marine group
25 NS9 marine group
52 NS10 marine group
17 Fluviicola
6 Ulvibacter
3 Formosa
91 Formosa
12 NS2b marine group
5 Flavobacteriaceae
84 NS5 marine group
40 NS5 marine group
47 NS4 marine group
34 NS4 marine group
24 NS4 marine group
55 NS4 marine group
37 NS4 marine group
11 NS5 marine group
132 NS5 marine group
23 Flavobacteriaceae
36 Polaribacter
15 Aurantivirga
39 NS7 marine group
88 NS7 marine group
33 Saprospiraceae
80 Pseudoalteromonas
54 SAR86
57 SAR86
118 SAR86
43 SAR86
38 SAR86
2 Psychrobacter
59 OM43
1 OM60(NOR5)
26 SAR92
63 SAR92
94 KI89A
95 Thiotrichaceae
7 Roseibacillus
Alphaproteobacteria
Actinobacteria
Gammaproteobacteria
Cytophagales
Flavobacteriales
Chitinophagales
Gammaproteobacteria
Verrucomicrobiales
M2 1 DNA
M2 2 DNA
M2 3 DNA
M1 DNA
M3 2 DNA
M3 3 DNA
M4 1 DNA
M4 2 DNA
M2 1 RNA
M2 2 RNA
M2 3 RNA
M1 RNA
M3 1 RNA
M3 3 RNA
M4 1 RNA
M4 2 RNA

Fig. S6

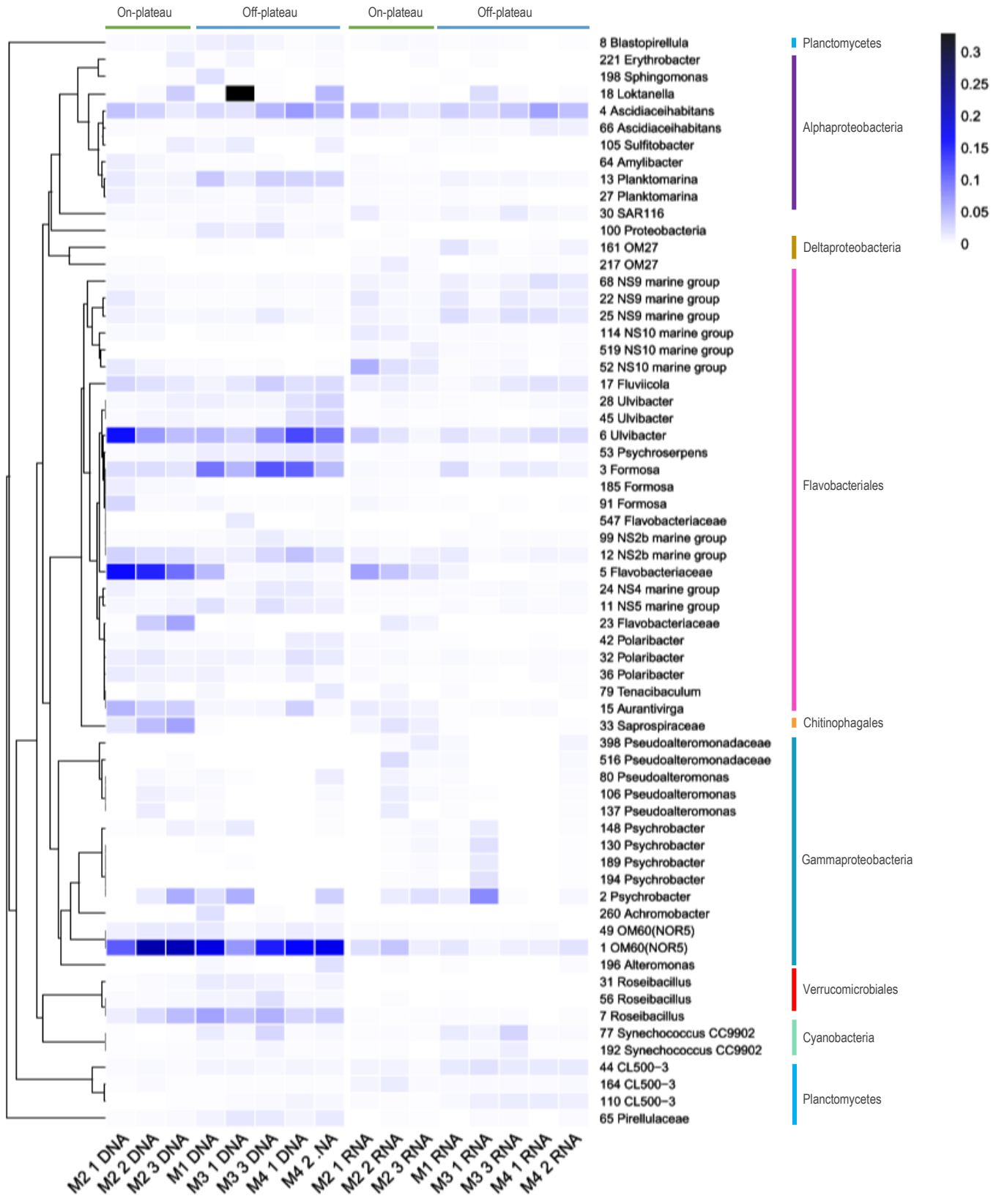
On-plateau
Off-plateau
On-plateau
Off-plateau
8 Blastopirellula
221 Erythrobacter
198 Sphingomonas
18 Loktanella
4 Ascidiaceihabitans
66 Ascidiaceihabitans
105 Sulfitobacter
64 Amylibacter
13 Planktomarina
27 Planktomarina
30 SAR116
100 Proteobacteria
161 OM27
217 OM27
68 NS9 marine group
22 NS9 marine group
25 NS9 marine group
114 NS10 marine group
519 NS10 marine group
52 NS10 marine group
17 Fluviicola
28 Ulvibacter
45 Ulvibacter
6 Ulvibacter
53 Psychroserpens
3 Formosa
185 Formosa
91 Formosa
547 Flavobacteriaceae
99 NS2b marine group
12 NS2b marine group
5 Flavobacteriaceae
24 NS4 marine group
11 NS5 marine group
23 Flavobacteriaceae
42 Polaribacter
32 Polaribacter
36 Polaribacter
79 Tenacibaculum
15 Aurantivirga
33 Saprospiraceae
398 Pseudoalteromonadaceae
516 Pseudoalteromonadaceae
80 Pseudoalteromonas
106 Pseudoalteromonas
137 Pseudoalteromonas
148 Psychrobacter
130 Psychrobacter
189 Psychrobacter
194 Psychrobacter
2 Psychrobacter
260 Achromobacter
49 OM60(NOR5)
1 OM60(NOR5)
196 Alteromonas
31 Roseibacillus
56 Roseibacillus
7 Roseibacillus
77 Synechococcus CC9902
192 Synechococcus CC9902
44 CL500−3
164 CL500−3
110 CL500−3
65 Pirellulaceae
Planctomycetes
Alphaproteobacteria
Deltaproteobacteria
Flavobacteriales
Chitinophagales
Gammaproteobacteria
Verrucomicrobiales
Cyanobacteria
Planctomycetes
0.3
0.25
0.2
0.15
0.1
0.05
0
M2 1 DNA
M2 2 DNA
M2 3 DNA
M1 DNA
M3 1 DNA
M3 3 DNA
M4 1 DNA
M4 2 NA
M2 1 RNA
M2 2 RNA
M2 3 RNA
M1 RNA
M3 1 RNA
M3 3 RNA
M4 1 RNA
M4 2 RNA

Fig. S7

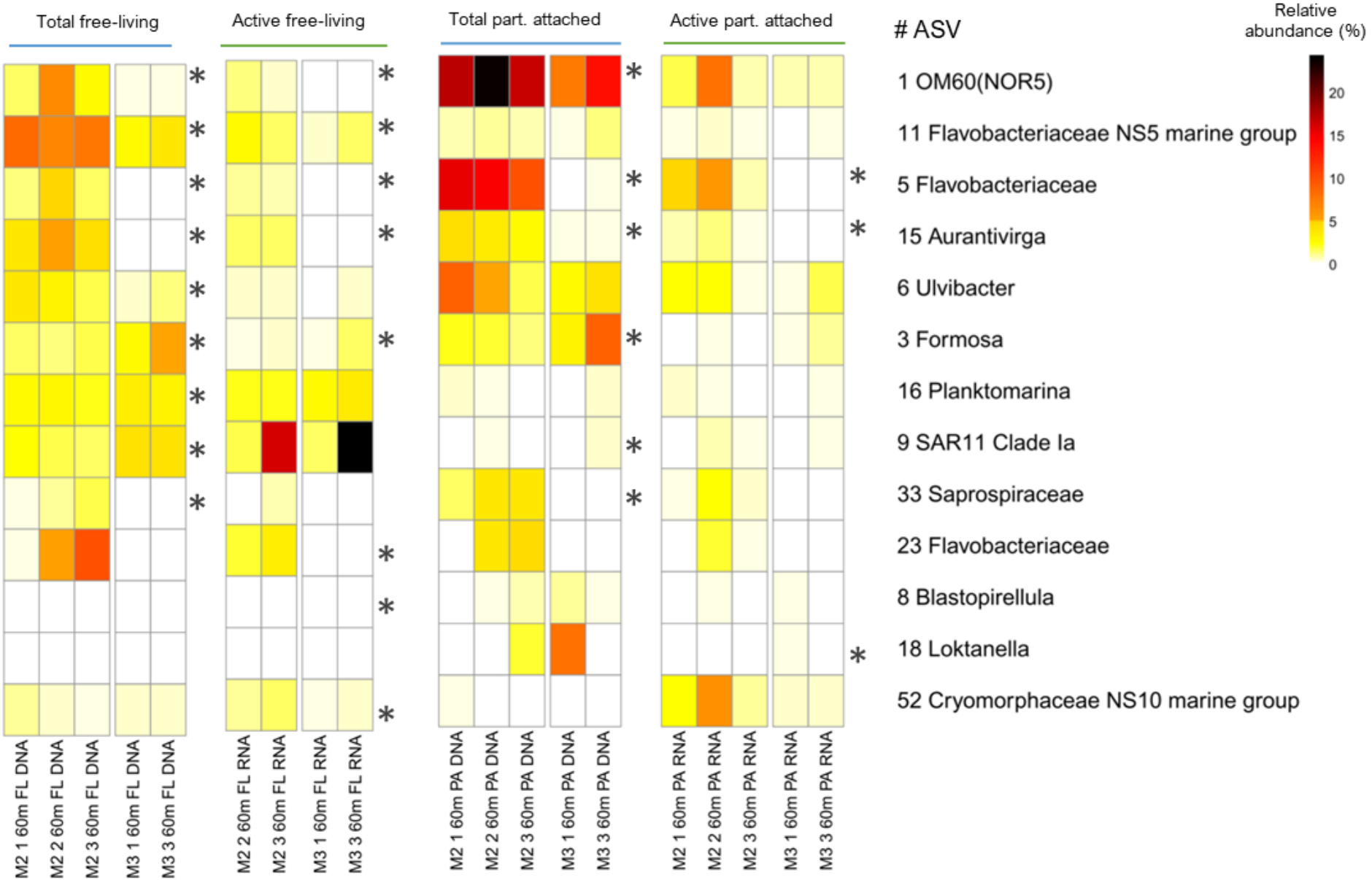
Total free-living
Active free-living
Total part. attached
Active part. attached
ASV
Relative abundance (%)
20
15
10
5
0
1 OM60(NOR5)
11 Flavobacteriaceae NS5 marine group
5 Flavobacteriaceae
15 Aurantivirga
6 Ulvibacter
3 Formosa
16 Planktomarina
9 SAR11 Clade Ia
33 Saprospiraceae
23 Flavobacteriaceae
8 Blastopirellula
18 Loktanella
52 Cryomorphaceae NS10 marine group
M2 1 60m FL DNA
M2 2 60m FL DNA
M2 3 60m FL DNA
M3 1 60m FL DNA
M3 3 60m FL DNA
M2 2 60m FL RNA
M2 3 60m FL RNA
M3 1 60m FL RNA
M3 3 60m FL RNA
M2 1 60m PA DNA
M2 2 60m PA DNA
M2 3 60m PA DNA
M3 1 60m PA DNA
M3 3 60m PA DNA
M2 1 60m PA RNA
M2 2 60m PA RNA
M2 3 60m PA RNA
M3 1 60m PA RNA
M3 3 60m PA RNA

Fig. S8

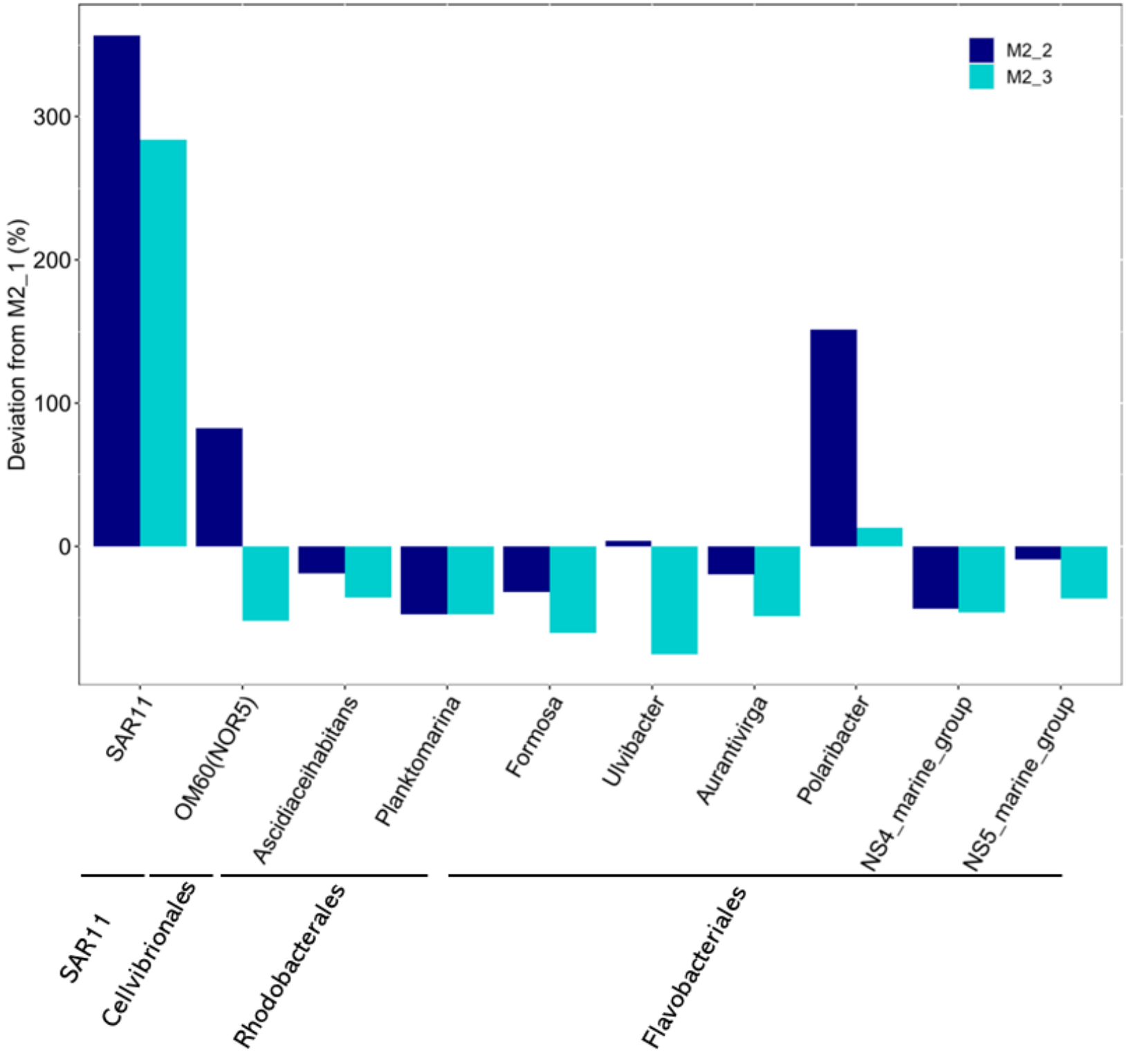
M2_2
M2_3
Deviation from M2_1 (%)
300
200
100
0
SAR11
OM60(NOR5)
Ascidiaceihabitans
Planktomarina
Formosa
Ulvibacter
Aurantivirga
Polaribacter
NS4_marine_group
NS5_marine_group
SAR11
Cellvibrionales
Rhodobacterales
Flavobacteriales

Fig. S9

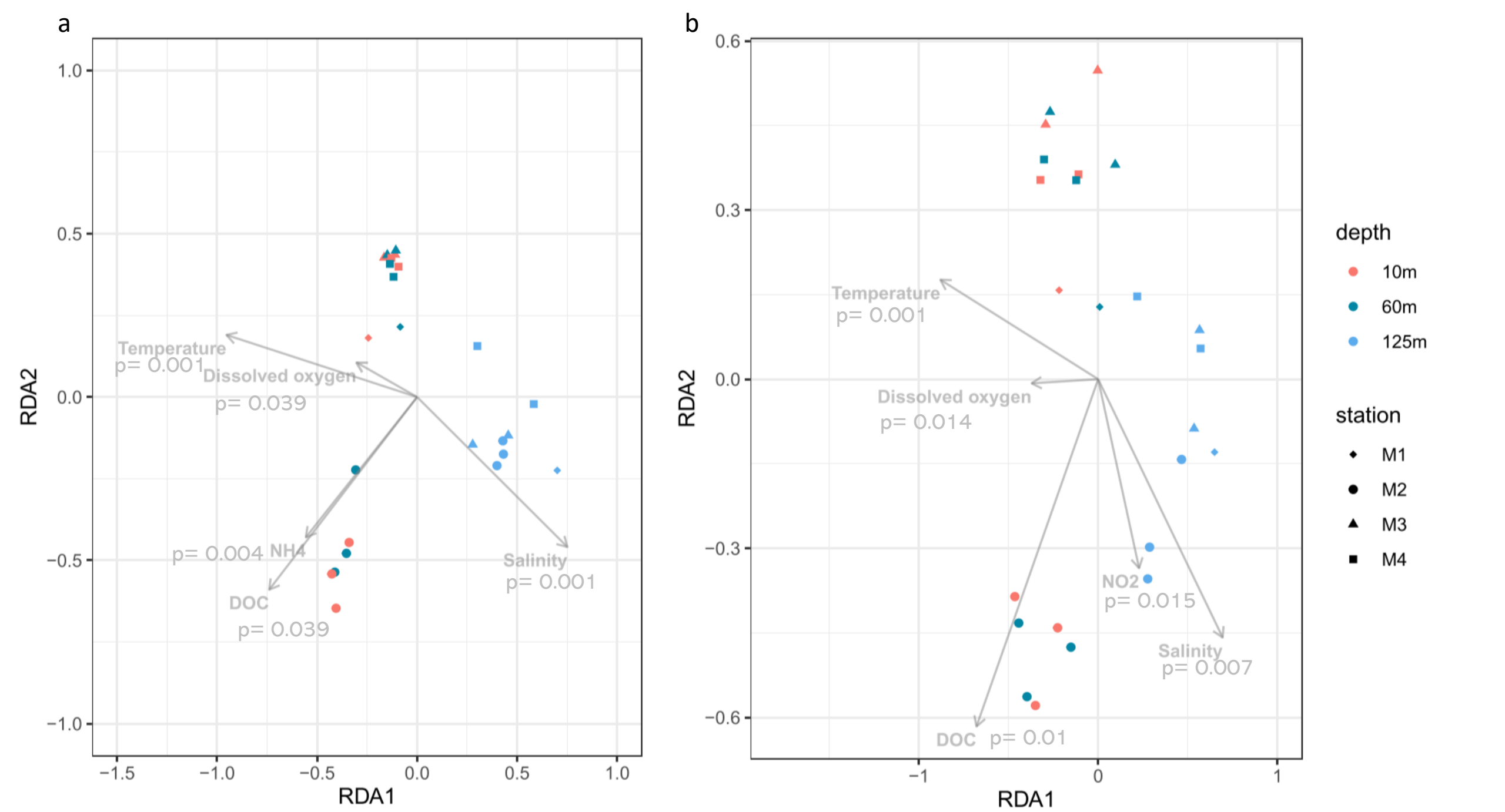
a
b
RDA1
RDA2
Temperature
p= 0.001
Dissolved oxygen
p= 0.039
p= 0.004 NH4
DOC
p= 0.039
Salinity
p= 0.001
Temperature
p= 0.001
Dissolved oxygen
p= 0.014
NO2
p= 0.015
Salinity
p= 0.007
DOC p= 0.01
depth
10m
60m
125m
station
M1
M2
M3
M4

Fig. S10

Supplementary Figures

Figure S1. Seasonal bloom dynamics for on-plateau station M2 and off-plateau stations M3 and M4. The green line indicates the 10-year climatological mean (2007-2017) of Chl *a* concentrations and its SD illustrated as the green shaded area. The blue line denotes Chl *a* concentrations for the year 2018 (MOBYDICK cruise). Chl *a* data are from Global Ocean Satellite Observations (Copernicus-GlobColour). Reprocessed data are provided by Copernicus Marine Service. The time period of the MOBYDICK cruise is marked with a rectangle. Note different scales of y-axis.

Figure S2. Depth profiles of temperature and density anomaly for the repeated visits at the 4 stations.

Figure S3. Depth profiles of DOC, prokaryotic abundances and Chl *a* at station M1.

Figure S4. Non-Metric Multidimensional Scaling (NMDS) of potentially active (RNA) prokaryotic communities in the (a) free-living and (b) particle-attached fraction from all depth layers based on Bray-Curtis Dissimilarity.

Figure S5. Relative abundance of potentially active (RNA) free-living (FL) and particle-attached (PA) taxa grouped at order level in surface waters (10 m). For stations M2, M3 and M4 the mean relative abundances of the repeated visits are shown.

Fig. S6. Relative abundance of ASVs with corresponding phylum (right colored sidebar) in the free-living fraction in surface waters (10 m). Only ASVs with >1% relative abundance in at least one sample are shown. On-plateau in green; off-plateau in blue. DNA: total community, RNA: potentially active community.

Fig. S7. Relative abundance of ASVs with corresponding phylum (right colored sidebar) in the particle-attached fraction in surface waters (10 m). Only ASVs with >1% relative abundance in at least one sample are shown. On-plateau in green; off-plateau in blue. DNA: total community, RNA: potentially active community.

Fig. S8. Relative abundance of ASVs that contribute significantly ($p<0.05$) to the dissimilarity between stations M2 and M3 (SIMPER analysis) at 60m. Asterisk highlight significant differences for a given ASV between sites, in either the free-living or particle-attached fractions, for the total (DNA) or potentially active (RNA) communities. Only the ASVs with relative abundance >5% in at least one of the samples are shown. Note that the ASVs that contribute to the difference among sites are not always the same for the total and the active communities

Fig. S9. Changes in the absolute abundance of dominant taxa (RNA, free-living fraction) between the first and the second (M2_3) and the first and the third (M2_3) visit at station M2 at 10 m. Deviations are given as percent; positive and negative values indicate an increase and a decrease, respectively, in abundance over the repeated visits at station M2. The deviation was calculated based on a formula published in Agogué et al (2011).

Fig. S10. Redundancy analysis of the total community (DNA-based dataset) in the free-living fraction (a) and particle attached (b). The significant environmental response-vectors are shown. Colors indicate water depths and symbol shapes correspond to sites. The variables were selected prior the RDA analysis (with variance inflation <10) excluding the redundant constraints.

Table S1. Percent prokaryotic cells in the 0.8 μm filtered seawater of cells in unfiltered seawater.

Station	Depth (m)	Fraction of cells in < 0.8 μm size fraction (%)
M1	15	115
M2-1	10	84
M2-2	10	93
M2-2	60	82
M2-3	60	79
M3-1	10	91
M3-1	60	83
M3-3	10	86
M3-3	60	83
M4-2	15	96

Table S2. Prokaryotic diversity as illustrated by the Observed, Shannon and Inverse Simpson Index for all depths and repeated visits at the 4 sites. NA – Not Available

Station	**M1**				**M2_1**				**M2_2**				**M2_3**				
Fraction	free-living DNA				free-living DNA				free-living DNA				free-living DNA				
Depth (m)	10	60	125	300	10	60	125	300	15	60	125	300	10	60	125	300	15
Observed	357	448	588	604	256	329	480	590	293	310	469	675	347	297	515	637	439
Shannon	4,630417587	4,911170603	5,016702863	5,1742284	4,050761314	4,519927552	4,973573443	5,324898909	4,199674721	4,321745361	4,923799894	5,39013288	4,557528066	4,376234884	5,036416351	5,372785124	5,005918554
InvSimpson	42,82129835	58,02194061	31,7209722	52,58309965	28,9092411	46,7586488	46,12942033	72,23921259	29,21192078	36,99498058	41,97304834	64,65604812	43,44739127	35,82888635	45,03269349	72,06032229	74,84599849
Station	**M1**				**M2_1**				**M2_2**				**M2_3**				
Fraction	attached DNA				attached DNA				attached DNA				attached DNA				
Depth (m)	10	60	125	300	10	60	125	300	15	60	125	300	10	60	125	300	15
Observed	282	283	545	866	259	231	290	439	273	231	334	704	347	297	515	637	439
Shannon	4,013059399	3,913617347	5,071673974	6,012926553	3,671495301	3,588997236	3,963424462	4,611143781	3,685029331	3,40815961	4,123871042	5,691295054	3,6529	3,538	3,796	3,9944	3,518
InvSimpson	18,41429539	19,21990533	47,68899127	178,9420594	14,55652021	13,95914847	20,17997005	32,94964122	12,69473407	10,4241389	20,2013473	118,7923767	14.21149175	10,4241389	20,2013473	118,7923767	8,177114762
Station	**M1**				**M2_1**				**M2_2**				**M2_3**				
Fraction	free-living RNA				free-living RNA				free-living RNA				free-living RNA				
Depth (m)	10	60	125	300	10	60	125	300	15	60	125	300	10	60	125	300	15
Observed	510	1107	1279	857	930	NA	1066	1031	467	953	680	948	513	569	1274	1346	1015
Shannon	4,391351947	6,26176654	6,553091444	5,643766982	6,043665186	NA	6,373004977	5,967207732	4,587999483	6,038872206	5,208954219	5,991221674	4,794227976	4,936724393	6,56084046	6,661230197	6,147218663
InvSimpson	12,47474901	199,7510742	236,2879011	31,81886256	170,37426	NA	284,3064592	40,76355835	23,92997487	161,2016865	41,25067073	111,66426	27,0774122	28,72407112	256,0138486	202,2292605	171,5273223
Station	**M1**				**M2_1**				**M2_2**				**M2_3**				
Fraction	attached RNA				attached RNA				attached RNA				attached RNA				
Depth (m)	10	60	125	300	10	60	125	300	15	60	125	300	10	60	125	300	15
Observed	896	990	961	1152	896	990	961	1152	866	363	443	1188	1023	860	1053	795	995
Shannon	5,79465954	5,95422116	6,189837213	6,454896518	5,79465954	5,95422116	6,189837213	6,454896518	5,886758741	4,507552806	5,030836167	6,340782925	6,373348086	5,849730962	6,215210067	4,897418311	6,044759366
InvSimpson	85,19544355	93,97085242	203,6656298	281,132465	85,19544355	93,97085242	203,6656298	281,132465	131,207044	39,15112692	69,59025164	86,48967977	298,7720653	82,54598082	157,5615963	11,48080568	105,1908396

M3_1			**M3_2**				**M4_1**				**M4_2**			
free-living DNA			free-living DNA				free-living DNA				free-living DNA			
60	125	300	15	60	125	300	10	60	125	300	15	60	125	300
457	438	774	416	396	519	659	382	388	495	684	412	419	618	694
5,119911706	5,003944767	5,569760803	4,886634643	4,766888034	5,033568653	5,378535363	4,769761755	4,761656847	5,104457433	5,448336438	4,902835399	4,892809069	4,943056375	5,444155036
86,28261896	72,41899328	79,1641964	65,26185117	59,56053611	47,57175899	66,88524437	61,40002813	61,24781921	69,85134114	63,62046237	69,68530427	70,01692317	27,79842907	65,40092231
M3_1			**M3_2**				**M4_1**				**M4_2**			
attached DNA			attached DNA				attached DNA				attached DNA			
60	125	300	15	60	125	300	10	60	125	300	15	60	125	300
457	438	774	288	298	315	771	243	267	366	669	275	306	267	707
3,286	3,6634	4,77	3,997718952	4,08066732	3,954872015	5,750910961	3,717988494	3,884385475	4,404890291	5,647105594	3,969754376	4,070741559	2,928439517	5,557859019
7,240784755	13,19206106	16,93033334	20,40416923	22,46182369	18,90960618	129,6652914	16,20826173	19,36629488	29,77360972	125,7471711	19,14907738	22,8616917	4,539264699	73,51675384
M3_1			**M3_2**				**M4_1**				**M4_2**			
free-living RNA			free-living RNA				free-living RNA				free-living RNA			
60	125	300	15	60	125	300	10	60	125	300	15	60	125	300
1103	680	1211	897	523	703	1033	816	945	1213	946	1027	572	1351	937
6,443330058	4,863603132	6,369838161	5,872947044	4,541682703	5,04721143	6,157978297	5,645590785	5,936458808	6,5245001	6,0079269	6,114155036	4,721951749	6,647294232	6,070729353
280,3100004	18,29747807	82,2504423	127,1842817	15,83392416	26,54139064	78,5280407	94,82600929	136,7852678	300,0499905	102,6859357	161,4269072	18,65007181	273,5372002	151,9662869
M3_1			**M3_2**				**M4_1**				**M4_2**			
attached RNA			attached RNA				attached RNA				attached RNA			
60	125	300	15	60	125	300	10	60	125	300	15	60	125	300
947	996	878	1088	1089	1116	1165	943	1038	1270	1098	1093	383	929	1243
5,914238798	6,20376749	5,761394155	6,281651595	6,284950066	6,390307622	6,365012264	6,038599251	6,21247134	6,563289489	6,293072004	6,295741049	4,636097191	5,793395001	6,469338878
81,74213719	141,1394363	75,05190811	191,8025779	173,4126956	181,1869336	103,1794949	130,9402697	177,3185809	247,1549593	95,5618546	196,6217623	40,27047017	67,49777923	159,5258776

Table S3. Partial Mantel tests for total (DNA) and potentially active (RNA) prokaryotic community composition, diatom community composition and environmental parameters. Rho values are shown. ** $p < 0.01$, * $p < 0.05$. Diatom community composition was determined by microscopic observations and the results are presented in Lafond et al. (2020)

	Prokaryotic Community Composition			
	Total		Active	
	Free-living	Particle-attached	Free-living	Particle-attached
Diatom community composition	0.6006 **	0.4498**	0.5257**	0.3682**
Combined environmental parameters	0.3525**	0.3003*	0.3969**	0.3126**
Temperature	0.2559**	0.3627**	0.5493**	0.3558**
Salinity	0.2553*	0.315**	0.4528**	0.2677**
Dissolved oxygen	0.2783*	0.257	0.3782*	0.2457*
NH_4^+	0.3668**	0.1354	0.1262	0.1222
PO_4^{3-}	0.08138	0.0796	0.114	0.1021
$Si(OH)_4$	0.4228**	0.4413**	0.6532**	0.4747**
NO_2^-	0.1993	0.2615*	0.3636*	0.2568*
NO_3^-	0.05504	0.05192	0.07594	0.07463
DOC	0.3153**	0.07243	-0.06333	0.1312

Hernandez et al. (JMarSyst)

Table S4. Environmental parameters used for the RDA anlayses.

Station	Depth (m)	Salinity	Temp (°C)	Oxygen (µM)	NH4+ (nM)	PO4 (µM)	Si(OH)4 (µM)	NO2 (µM)	NO3 (µM)	Chlorophyll_c3 (µg/L)	Peridinin (µg/L)	Fucoxanthin (µg/L)	Prasinoxanthin (µg/L)	19'-Hexanoyloxyfucoxanthin (µg/L)	Alloxanthin (µg/L)	Zeaxanthin (µg/L)	Lutein(µg/L)	Chlb (µg/L)	Chlorophyll_a (µg/L)	Phaeophytin_a (µg/L)	POC (µM)	PON (µM)
M1	25	33,89	5,08	322,04	421	1,63	6,49	0,28	24,76	0,0378	0,0045	0,0738	0,0021	0,1285	0,0023	0.0018	0,0008	0,0096	0,3111	0,0019	4,838	0,863
M1	50	33,89	4,90	320,48	712	1,67	6,9	0,29	24,55	0,0514	0,005	0,0939	0,0035	0,1428	0,0037	0.0016	0,0013	0,0178	0,3633	0,0025	4,964	0,855
M1	125	34,01	1,97	296,44	0	2,15	30,02	0,03	31,47	0,0015	0,0023	0,0116	0	0,0013	0,0004	0	0	0	0,0173	0,0036	1,511	0,234
M1	250	34,22	2,21	231,95	0	2,3	47,63	0,04	34,45	0,0004	0,0012	0,0025	0	0	0	0	0	0	0,0035	0,0022	0,907	0,174
M2_1	9	33,86	5,17	322,09	704	1,45	1,17	0,27	21,62	0,0346	0,0103	0,077	0,0027	0,0921	0,0031	0.0048	0,0015	0,0109	0,2795	0,003	5,531	0,88
M2_1	48	33,87	5,08	320,83	729	1,45	1,14	0,27	21,68	0,0416	0,0124	0,0854	0,0022	0,1013	0,0032	0.0046	0,002	0,0105	0,2886	0,0031	5,481	0,837
M2_1	124	33,93	1,88	325,59	642	2,07	22,85	0,37	28,96	0,0038	0,0057	0,0674	0	0	0	0.0006	0,0004	0	0,128	0,0149	3,447	0,382
M2_1	349	34,25	2,08	231,70	0	2,33	51,44	0,03	36,89	0,0003	0	0,0046	0	0	0	0	0	0	0,006	0,0048	3,662	0,288
M2_2	15	33,87	5,24	316,00	1090	1,47	1,29	0,3	21,25	0,0431	0,008	0,1124	0,0059	0,0743	0,0037	0.004	0,001	0,0223	0,3246	0,0025	4,437	0,691
M2_2	50	33,86	5,24	316,15	1106	1,48	1,35	0,27	21,38	0,0429	0,0083	0,114	0,0059	0,0751	0,0038	0.004	0,0011	0,0227	0,3336	0,0024	3,541	0,544
M2_2	125	33,93	2,23	319,25	297	2,05	21,69	0,32	28,95	0,0044	0	0,034	0	0,0037	0	0.0004	0,0007	0	0,0561	0,0118	2,178	0,315
M2_2	350	34,25	2,06	230,07	0	2,47	51,65	0,03	34,57	0,0003	0	0,0041	0	0	0	0.0002	0	0	0,005	0,0054	1,161	0,153
M2_3	15	33,86	5,18	318,82	899	1,51	2,6	0,3	21,75	0,0761	0,0125	0,216	0,0184	0,1033	0,0049	0.0047	0,0013	0,0519	0,575	0,0045	5,915	0,933
M2_3	50	33,86	5,07	317,59	957	1,49	2,67	0,3	21,61	0,0914	0,0173	0,2356	0,0167	0,1239	0,0063	0.0043	0,0015	0,0534	0,6218	0,0061	5,984	0,966
M2_3	127	33,95	2,11	315,71	263	2,06	23,5	0,32	28,91	0,0026	0,002	0,0212	0	0,0025	0	0.0003	0,0005	0	0,0347	0,0079	1,728	0,26
M2_3	351	34,31	2,15	214,34	0	2,34	56,46	0,04	34,56	0,0002	0	0,0033	0	0	0	0	0	0	0,0041	0,0045	1,034	0,14
M3_1	25	33,82	5,60	314,77	501	1,62	2,31	0,24	23,39	0,0256	0,0049	0,034	0	0,1041	0,0013	0.0014	0	0,0073	0,191	0	4,262	0,719
M3_1	50	33,82	5,60	314,67	508	1,62	2,31	0,24	23,27	0,0256	0,0051	0,0343	0	0,1013	0,0013	0.0014	0	0,0072	0,1892	0	4,05	0,704
M3_1	125	33,87	2,72	316,75	503	1,99	18,01	0,4	28,04	0,0281	0,0056	0,0372	0	0,0502	0	0.0007	0	0,0019	0,1152	0,0062	2,288	0,347
M3_1	250	34,06	2,23	276,04	0	2,15	34,58	0,02	32,05	0,0006	0	0,0027	0	0	0	0	0	0	0,0045	0,0018	0,998	0,187
M3_3	24	33,81	5,32	312,90	722	0,01	2,42	0,01	0,02	0,0189	0,0045	0,029	0	0,065	0,0012	0.0006	0,0003	0,0054	0,1402	0	3,297	0,547
M3_3	49	33,81	5,32	313,27	733	1,61	2,45	0,23	23,02	0,0193	0,0043	0,0292	0	0,0657	0,0012	0.0006	0,0003	0,0056	0,1413	0	3,117	0,525
M3_3	126	33,90	2,71	313,79	246	2,01	20,67	0,38	28,19	0,0119	0,0054	0,0222	0	0,0177	0	0.0004	0	0,001	0,0625	0,0052	1,644	0,254
M3_3	249	34,03	2,21	285,48	0	2,1	32,31	0,02	30,97	0,0009	0,0004	0,0046	0	0	0	0.0002	0	0	0,0067	0,0024	0,903	0,127
M4_1	23	33,85	4,50	324,05	354	1,72	4,13	0,25	25,5	0,0231	0,0039	0,0483	0	0,0832	0,0011	0.0014	0,0004	0,003	0,1801	0	3,853	0,646
M4_1	48	33,85	4,48	323,24	349	1,68	4,19	0,25	25,5	0,0233	0,0037	0,0547	0	0,079	0,0011	0.0016	0,0005	0,0029	0,1811	0	4,414	0,691
M4_1	124	33,91	2,83	324,06	812	1,94	18,85	0,28	27,57	0,0221	0,0024	0,0739	0	0,0154	0	0.0009	0,0007	0,001	0,1158	0,0064	2,932	0,43
M4_1	251	34,07	1,73	287,82	0	2,13	36,83	0,01	32,17	0,001	0	0,0043	0	0,0005	0	0.0003	0	0	0,006	0,0026	1,194	0,17
M4_2	24	33,85	4,46	320,13	481	1,71	4,8	0,27	24,79	0,0278	0,003	0,0658	0	0,0857	0,0012	0.0009	0,0006	0,0038	0,2151	0,0013	3,745	0,564
M4_2	52	33,85	4,46	320,23	495	1,71	4,8	0,27	24,27	0,0275	0,0033	0,0641	0	0,0847	0,0012	0.0009	0,0007	0,0037	0,2078	0	3,536	0,58
M4_2	125	33,91	2,56	320,07	930	1,99	20,54	0,35	26,91	0,0141	0,0015	0,0408	0	0,0186	0	0.0005	0,0003	0,0047	0,0785	0,0035	2,074	0,329
M4_2	246	34,07	1,96	282,39	0	2,13	34,66	0,04	30,94	0,0006	0,0012	0,0033	0	0	0	0	0	0	0,0056	0,0021	1,136	0,153

DOC (µM)	Prokaryotic Abundance (cells /mL)	Photosynthetic Pico-Nanoeukaryotes (cells/mL)*	Heterotrophic Nanoflagellates (cells /mL)*	Viral like particles (VLPs/mL)*	Bacterial Production (µg C/L/h)*
50,3	606000	8040	943	3,10E+06	21,54
50,3	619000	8010	964	3,69E+06	18,04
48,1	253000	38,5	366	2,05E+06	1,97
46,2	222000	25,2	168	1,28E+06	1
52,5	1180000	3190	1340	4810000	22,16
53,4	1150000	2770	1700	5850000	30,99
49,8	371000	41,5	466	2110000	5,01
46,8	269000	16,3	257	1170000	1,37
54,6	837000	3770	2840	8,02E+06	46,23
56,7	794000	3490	2910	7,11E+06	35,81
49	367000	80	726	2,94E+06	4,59
46,8	220000	13,3	278	1,31E+06	1,3
54,6	665000	8130	1730	7,40E+06	56,91
55	708000	8410	1890	7,27E+06	45,09
49	301000	56,1	551	2,43E+06	3,58
45,9	214000	14,8	300	1,09E+06	1,27
50,4	696000	3720	625	3,64E+06	15,59
50,2	665000	3590	763	3,65E+06	14,39
47	358000	42,8	655	2,40E+06	4,5
44,2	191000	7,38	222	1,52E+06	0,41
49,1	446000	1490	847	4,10E+06	13,18
52	445000	1520	798	3,71E+06	13,76
49,4	325000	33,9	931	2,83E+06	3,62
44,2	205000	10,3	362	2,25E+06	1,69
49,3	552000	3180	851	3,45E+06	13,98
50	550000	3160	965	3,80E+06	13,1
49,4	440000	220	655	3,00E+06	6,82
44,9	193000	8,4	178	1,43E+06	0,3
49,5	501000	3700	884	3320000	14,39
51,2	506000	3760	889	3060000	14,81
50	388000	104	658	2740000	5,56
44,9	199000	4,2	301	1390000	0,51